Chemosphere 254 (2020) 126857

Contents lists available at ScienceDirect

Chemosphere

journal homepage: www.elsevier.com/locate/chemosphere

Radiological and pollution risk assessments of terrestrial radionuclides and heavy metals in a mineralized zone of the siwalik region (India)

Pragya Pandit [a, *], Preeti Mangala [a], Atul Saini [b], Pargin Bangotra [c], Vinod Kumar [d], Rohit Mehra [e], Dibakar Ghosh [a]

[a] Atomic Minerals Directorate for Exploration and Research, New Delhi, 110066, India
[b] Department of Geography, Delhi School of Economics, University of Delhi, Delhi, 110007, India
[c] Material Research Laboratory, Deptt of Physics, SBSR, Sharda University, Greater Noida, 201310, India
[d] Department of Botany, Government Degree College, Ramban, 182144, India
[e] B. R. Ambedkar National Institute of Technology, Jalandhar, 144011, India

HIGHLIGHTS

- 218 samples from 33 locations in a uranium-mineralized area of Siwaliks were studied for radiological and pollution risk assessment.
- Concentrations and distributions of radionuclides and heavy metals were correlated with sediment physico-chemical parameters.
- Majority of radiation hazard indices were above the world average value.
- Non-carcinogenic and carcinogenic risks for both children and adults were below EPA threshold limits.
- Spatial distributions of radionuclides and heavy metals indicated precipitation towards south of the clay oxidizing zone.

ARTICLE INFO

Article history:
Received 9 October 2019
Received in revised form
8 April 2020
Accepted 19 April 2020
Available online 22 April 2020

Handling Editor: Martine Leermakers

Keywords:
Hazard indices
Radioactivity
Gamma radiation survey
Gamma spectrometry
Spatial mapping

ABSTRACT

The present study reveals the distribution of terrestrial radionuclides (^{226}Ra, ^{232}Th and ^{40}K) and heavy metals (Cr, Ni, Cu, Zn, Pb, Co) from soil samples of Una, Hamirpur and Kangra districts of Himachal Pradesh (India). The ^{226}Ra, ^{232}Th, ^{40}K activity concentration in the studied region has been varied from 8 to 3593 Bq kg^{-1}; 21–370 Bq kg^{-1}16; 62–7130 Bq kg^{-1} respectively. High disequilibrium factor (^{238}U/^{226}Ra) depicts that uranium constantly migrates from clay oxidizing zone and getting precipitated with enrichment towards south. An attempt has been made to correlate the distribution of these radionuclides and heavy metals with geology and rock type formation of Siwalik region. The concentration of Pb, Zn and Co was found higher than Indian average background value. Multiple radiological and pollution indices have been estimated for proper risk analysis in the studied region. The annual effective dose in studied region is lower than the recommended limit of 1.0 mSv a^{-1}. The obtained geo-accumulation index and enrichment factor indicated that the sites located in the Hamirpur and Kangra regions were moderately contaminated with Pb and Co. The Nemerow pollution index and contamination security index suggested that almost 45% sites were slightly to moderately polluted. The non-carcinogenic and carcinogenic risks for both children and adults were within acceptable limits.

1. Introduction

Radionuclides and heavy metals are high-risk pollutants and are ubiquitously present in ecosystem (Salmanighabeshi et al., 2015). Soil is an extremely heterogeneous system that acts as source and sinks for radionuclides, inorganic and organic pollutants (Saha et al., 2017; Wu et al., 2018). Radionuclides and heavy metals can accumulate in the soil depending on the physicochemical properties (organic matter, pH, cationic and anionic exchange capacity) and land use pattern (agricultural, mining, industrial or urban (Hao et al., 2014; Zhang et al., 2019). The heavy metals are highly toxic

* Corresponding author.
E-mail address: pragyapandit.amd@gov.in (P. Pandit).

https://doi.org/10.1016/j.chemosphere.2020.126857
0045-6535/

due to their non-biodegradable nature, persistence, biomagnification and bioaccumulation properties, However radionuclides remain in soil for relatively long periods, owing to their large half-lives and contribute significant dose to mankind (Luo et al., 2011; Bangotra et al., 2019; Gasiorek et al., 2017). The exposure of heavy metals and radionuclides through different pathways can cause neurotic disorder, kidney dysfunction, risk of leukemia and cancer to different organs (melanoma, kidney and prostate) (ICRP, 2017; United Nations Scientific Committee on the Effect of Atomic Radiation (UNSCEAR), 2000). Furthermore in uranium mining sites, biotoxic heavy metal contaminants coexist with radioactive ones and it is necessary to evaluate the cumulative impact of multiple contaminants and natural stressors for realistic risk assessment (Cuvier et al., 2016; Singh et al., 2018).

Siwalik region in Himachal Pradesh is one of the main uranium prospecting regions of AMD. Strategically, AGRS and heavy metal analysis are regularly conducted at the preliminary stages of uranium prospecting to delineate and identify radiation anomalies and provide baseline environmental monitoring data for AMD study areas. A detailed ground based radiometric survey led to the initiation of exploratory mining at Andalada in Siwaliks, which has resulted in the delineation of six discontinuous ore lenses with dimensions of 300 × 100 m and thicknesses of 0.98–2.2 m. In that area, a proven reserve of 3058 tons containing 0.02–0.045% of U_3O_8 (2.32 tons) was identified (Kaul et al., 1979). Numerous studies have been conducted on health risk assessment, environmental contamination and toxicity due to different radionuclides and heavy metals in various mining areas in India and world (Mkandawire and Deudel, 2005; Popic et al., 2011; Belayaeva et al., 2019) but, no study on risk assessment so far has been performed in the Siwalik region.

In this manuscript, a comprehensive ecological and radiological risk assessment has been carried out and degree of pollution has been assessed in studied region, using geo-accumulation index (I_{geo}), enrichment Factor (EF), Nemerow Pollution Index ($PI_{nemerow}$), potential ecological risk (RI), contamination security index (CSI), air absorbed dose rate (D ($nGyh^{-1}$)), annual effective dose equivalent (AEDE) and excess lifetime cancer risk (ELCR). The carcinogenic and non-carcinogenic risks have been evaluated for human health risk assessment. The spatial distribution of radionuclides and heavy metals has been studied in order to understand the proper migration and further correlated with the geology of the region by conducting multivariate statistical analysis.

2. Materials and methodology

2.1. Regional geology and description of study site

The study region was located in the Siwalik sediments of Una (31°28′48″N, 76°16′48″E), Hamirpur (31°40′48″N, 76°31′12″E) and Kangra (32°06′00″N, 76°16′12″E) districts of Himachal Pradesh. The elevation of the study region varied from 369 to 1189 m. According to 2011 census, the populations of Una, Hamipur, and Kangra districts are 0.52, 0.46 and 1.51 millions, respectively. The average rainfall in the study area ranges from 290 to 380 cm. The soil found in the districts of Una, Hamirpur and Kangra are brown, alluvial and grey brown podzolic. Geologically, Siwalik sediments with thicknesses of around 6000 m are deposited along the foreland basins of Himalayas and considered a favorable host for the epigenetic sandstone type of uranium mineralization. The rocks of Siwalik Group are divided into the upper, middle and lower Siwaliks. The area of the present study falls within the Kangra sub-basin of the middle and upper Siwaliks. The northern boundary of the region is defined by the Main Boundary Thrust and its southern boundary is surrounded by the Himalayan Frontal Thrust. A number of radioactive anomalies in this basin were the focus of several studies on radiation hazards and the presence of heavy metals (Kaul et al., 1979, 1993). Radioactivity in the study area is hosted by pebbly sandstone conglomerates and uranium mostly exists in the form of an adsorbed phase within mud clasts, coaly matter, and clay minerals. The geological map of Siwaliks and location map utilized in the present study are shown in Fig. 1(a) and (b) respectively.

The study covered sub regions of Purohitan, Polion, Khawariyan, Kachhan and Dadoh in Una. Galotnala and Loharkar were the areas spanned in Hamirpur whereas, Kangra constituted Ghamirkhand, Manwala, Dhanotanala and Dhuli Bhatwan. The details of the sampling area (latitude, longitude, geological parameters and gamma dose rate) are listed in Table S1.

2.2. Sample collection and analysis

A total of 218 soil samples where 139 samples were collected from the Una (S_1–S_{16}), 34 samples from Hamirpur (S_{17}–S_{24}) and 45 samples from Kangra (S_{25}–S_{33}) districts of Himachal Pradesh during the period of 2016–2017. The soil samples (0.25 kg) were collected at a depth of 20 cm from the surface and homogenized, pulverized and sieved through −150 μ sized mesh. Quantitative

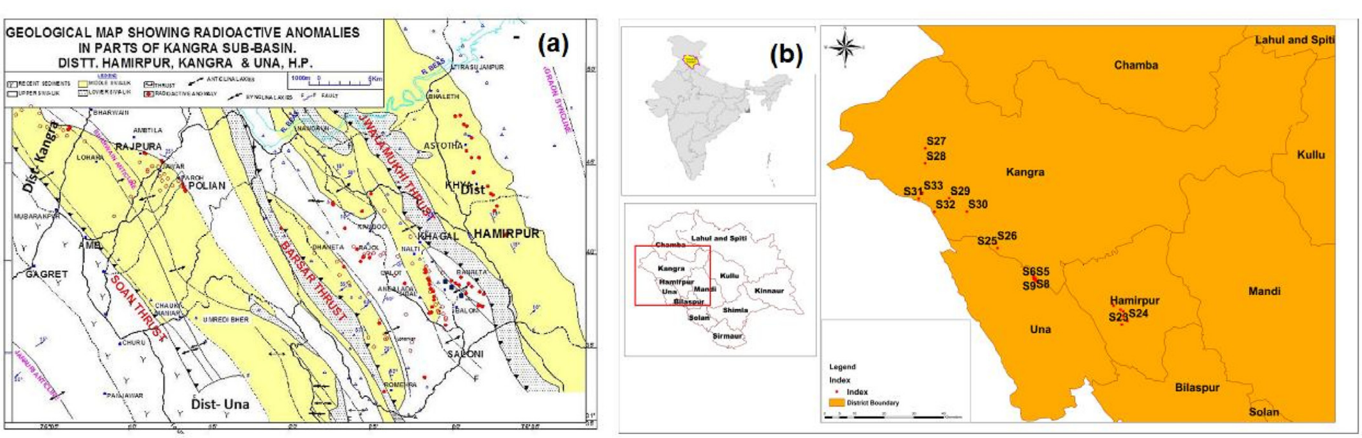

Fig. 1. (a) Geological map of Siwalik region (b) Sampling locations in Una, Hamirpur and Kangra districts of Himachal Pradesh, India.

determination of ^{226}Ra, ^{232}Th and ^{40}K was performed by gamma ray spectrometric system using NaI(Tl) gamma detector coupled with photomultiplier tube and a DSP based 2K MCA system. The gamma ray detector (5″ x 4″) has an active volume of 1286.38 cm^3, a resolution of 9.5% and an efficiency of 14.5% at 662 keV (^{137}Cs). A RSM was used to measure the gamma exposure rates (air absorbed dose rates) at the sampling sites. The survey meter was equipped with the 1" × 2" NaI (Tl) detector and calibrated by ^{137}Cs source. An arithmetic mean of the results of five measurements conducted at a height of 1 m was calculated to determine the gamma dose rate. Concentrations of heavy metals Cr, Ni, Co, Cu, Zn, and Pb were measured by wavelength dispersive X-ray fluorescence spectrometer (MagiX-Pro:PW2440, Panalytical, Neitherlands) after pelletizing the sample. The accuracy and precision achieved by WDXRF for Cr, Ni, Cu, Zn, Pb and Co was within 4% and 3%. The limit of detection (LOD) for Cr, Ni, Zn and Pb was 2 mg/kg, for Cu and Co was 3 $mgkg^{-1}$. The organic matter was determined by Walkley–Black chromic acid wet digestion method. pH was measured by a pH meter (Hanna HI98121).

2.3. Radiological hazard estimation

The most commonly used radiological hazard parameters air absorbed dose rate $(D(nGyh^{-1}))$, annual effective dose equivalent (AEDE), external (H_{ex}) and internal (H_{in}) hazards indices, gamma level index (I_γ)and excess lifetime cancer risk (ELCR) were estimated as per the methodology. (Beretka and Matthew, 1985; Örgün et al., 2007; Saito and Jacob, 1995; United Nations Scientific Committee on the Effect of Atomic Radiation (UNSCEAR), 2000; European Commission on Radiation Protection (ECRP), 1999) (Table S2).

2.4. Quantification of pollution and ecological risks

The comprehensive soil pollution assessment and environmental risk assessment was carried out by multiple pollution indices defined in the literature, I_{geo} (Muller, 1969), EF (Sutherland, 2000), Nemerow pollution index ($PI_{nemerow}$) (Zhong et al., 2010), Hakanson's ecological risk index (RI) (Håkanson, 1980) and contamination security index (CSI) (Pejman et al., 2015) (Table S3).

2.5. Human health risk assessment

The non-carcinogenic risks in the Siwalik region were evaluated based on the risk assessment model proposed by the U.S. Environmental Protection Agency (U.S. Environmental Protection Agency (US EPA), 1986; 1989, 2001). The exposures to different pollutants (chronic daily intakes) were calculated from the average daily doses of ingestion $Dose_{ing}(mgkg^{-1}d^{-1})$) inhalation $Dose_h(mgkg^{-1}d^{-1})$ and dermal contact $Dose_{derm}(mgkg^{-1}d^{-1})$ (U.S. Environmental Protection Agency (US EPA), 1986). The non-carcinogenic risk due to a particular metal, hazard quotient (HQ) was estimated as the ratio of the chronic daily exposure to the toxicity threshold (RfD). Further, hazard index (HI) was used for the assessment of the total non-carcinogenic effect; it represented the sum of individual HQ values determined for multiple heavy metals (U.S. Environmental Protection Agency (US EPA), 1986; Li et al., 2014). The corresponding formulas and chronic daily uptake parameters of exposure HQ and HI are listed in Table S4 (Ferreira-Baptista and De Miguel, 2005).

In this study, Cr, Ni, Pb and Co is considered carcinogens as per IARC (International Agency for Research on Cancer) and IRIS (Integrated Risk Information System) classification. Carcinogenic risk (CR) and total carcinogenic risk (TCR) values in the studied region were estimated using the methodology outlined in Table S4. The dose is multiplied by the corresponding slope factor (SF) to produce CR (Ferreira-Baptista and De Miguel, 2005).

2.6. Spatial distribution maps

The spatial distributions maps of radionuclides, heavy metals and corresponding radiological and pollution risks were prepared by ARCGIS software (Version 10.3, ESRI, California USA) and surfer 11 (Golden Software LLC, Colorado, USA).

2.7. Statistical analysis

The statistical analysis was done by utilizing Statistical Program for Social Science (SPSS, version 20). The geoelemental values of radiation hazard parameters and heavy metals were presented by AM, GM and R. The dispersion in the parameters was expressed by SD and IQR. The normality of the data was tested using S–W test. Pearson correlation analysis was performed to find correlation among radionuclides and heavy metals. Principal component analysis (PCA) and Factor analysis (FA) was performed for source identification of heavy metals and radionuclides. Linear regression analysis was carried out to find correlation between sediment physicochemical properties and heavy metals. All tests were conducted at a 95% confidence interval and values of $p < 0.05$ and $p < 0.001$ were considered statistically significant.

3. Results and discussion

3.1. Radioactivity measurements

3.1.1. Soil radioactivity (^{226}Ra, ^{232}Th and ^{40}K) and spatial distribution of radionuclides

The geo-elemental radioactivity concentrations of ^{226}Ra, ^{232}Th and ^{40}K in the Una, Hamirpur, and Kangra regions are listed in Table 1. Concentration of ^{226}Ra, ^{232}Th and ^{40}K in the Una region varied from 8 to 3593 Bq kg^{-1}, from 21 to 370 Bq $kg^{-1}$and from 217 to 7130 Bq kg^{-1} with mean values of 433, 66 and 764 Bq kg^{-1}, respectively. Fig. 2(a–c) demonstrate the graphical illustrations of the activity concentrations of ^{226}Ra, ^{232}Th and ^{40}K in the study region. Fig. 2(a) shows the relatively high variations of ^{226}Ra activity, Dadoh west exhibiting minimum and Polion east showing maximum in the Una region. The presence of grey sandstone rock without mudstone is responsible for the low uranium content in Dadoh west. However, Polion east contains medium to fine sandstone bedrocks with silt laminae and matrix-supported conglomerate mudstones that promote uranium adsorption. In the Hamirpur region, the concentrations of ^{226}Ra, ^{232}Th and ^{40}K varied from 43 to 3603 Bq kg^{-1}, from 21 to 102 Bq kg^{-1} and from 62 to 2449 Bq $kg^{-1}$with mean values of 818, 65 and 754 Bq kg^{-1} respectively. In the middle Siwalik region (composed of brown coarsely grained pebbly sandstone), a very high ^{226}Ra concentration (6833 Bq kg^{-1}) was observed at the S_{21} sampling site (Loharkar old) as it lied between the Jwalamukhi and Barsar thrusts and represented a transition zone between the middle and upper Siwaliks, as shown in Fig. 2(d–f). The sandstone type of uranium mineralization is associated with mudstone beds, which are observed in highly alkaline depositional environments and host radionuclides.

The activity concentrations of ^{226}Ra, ^{232}Th and ^{40}K in the Kangra region varied from 122 to 2009 Bq kg^{-1}, from 41 to 100 Bq kg^{-1} and 558–2449 Bq $kg^{-1}$with mean values of 789, 67 and 815 Bq kg^{-1}, respectively Fig. 2(g–i). A high ^{226}Ra activity concentration (1933 Bq kg^{-1}) was detected in the Dhuli Bhatawan area (S25) as the region is bounded by the Soan thrust in the west and Barsar thrust

Table 1
Descriptive statistics of the radionuclide concentrations and radiological hazard indices in the studied area (n = 218).

Parameters	Region	Mean	Median	GM	Variance	S.D.	Min	Max	R	IQR	S_k	ϰ
Ra ($Bq\cdot kg^{-1}$)	Una	432.98	129.31	160.06	478825.02	691.97	7.77	3593.07	3585.30	415.80	2.48	6.10
	Hamirpur	818.22	614.94	564.52	495653.61	704.02	43.29	3603.06	3559.77	779.75	1.96	5.08
	Kangra	789.10	577.22	629.13	272143.2	521.87	121.89	2009.10	1887.21	769.23	0.821	−0.37
Th ($Bq\cdot kg^{-1}$)	Una	66.30	62.11	61.68	1149.30	33.90	21.11	369.94	348.83	21.86	5.71	47.85
	Hamirpur	65.04	60.90	62.39	334.09	18.27	20.70	101.90	81.20	28.72	0.30	−0.25
	Kangra	66.80	60.90	64.57	320.46	17.90	41.41	100.20	58.87	30.85	0.492	−1.02
K ($Bq\cdot kg^{-1}$)	Una	764.29	713.00	698.53	342648.16	585.36	217	7130	6913	217.00	9.65	105.31
	Hamirpur	753.86	744.00	676.08	103017.98	320.96	62	2499	2387	186.00	3.09	18.80
	Kangra	814.55	744.00	779.04	111606.18	334.07	558	2449	1891	140.00	4.43	22.07
D ($nGyh^{-1}$)	Una	272.55	133.06	179.87	101855.61	319.14	52.67	1722.38	1669.71	198.60	2.45	5.84
	Hamirpur	448.93	356.67	334.57	105235.58	324.40	87.96	1741.33	1653.37	371.40	1.98	5.21
	Kangra	407.47	384.17	380.37	57200.39	239.16	135.20	985.60	850.64	368.60	0.77	−0.49
AEDE indoor ($mSvy^{-1}$)	Una	1.33	0.65	0.88	2.45	1.56	0.26	8.45	8.19	0.97	2.45	5.85
	Hamirpur	2.20	1.75	1.77	2.53	1.59	0.43	8.54	8.11	1.82	1.98	5.21
	Kangra	2.15	1.71	1.86	1.33	1.17	0.66	4.38	4.17	1.80	0.77	−0.49
AEDE outdoor ($mSvy^{-1}$)	Una	0.33	0.16	0.22	0.15	0.39	0.06	2.11	2.05	0.23	2.45	5.86
	Hamirpur	0.55	0.44	0.44	0.16	0.39	0.11	2.14	2.03	0.45	1.99	5.27
	Kangra	0.53	0.43	0.46	0.086	0.29	0.17	1.21	1.04	0.45	0.78	−0.47
H_{in}	Una	2.74	1.09	1.52	13.99	3.74	0.25	19.79	19.44	2.19	2.47	5.97
	Hamirpur	4.80	3.73	3.68	3.80	14.46	0.62	19.94	19.32	4.37	1.97	5.16
	Kangra	4.69	3.56	3.92	7.89	2.80	1.10	11.19	10.09	4.29	0.79	−0.49
H_{ex}	Una	1.58	0.77	1.03	3.50	1.87	0.31	10.08	9.77	1.16	2.45	5.85
	Hamirpur	2.61	2.08	2.11	3.62	1.90	0.50	10.20	9.70	2.17	1.98	5.22
	Kangra	2.55	2.03	2.21	1.96	1.40	0.77	5.76	4.99	2.16	0.77	−0.43
$I\gamma$	Una	4.05	2.05	2.74	13.99	3.74	0.83	25.01	24.18	2.85	2.44	5.81
	Hamirpur	6.60	5.28	5.38	22.01	4.69	1.38	25.31	23.93	5.36	1.98	5.22
	Kangra	6.47	5.18	5.63	11.95	3.45	2.08	14.35	12.27	5.34	0.76	−0.50
ELCR	Una	1.17	0.56	0.77	1.87	1.36	0.21	7.39	7.18	0.83	2.45	5.36
	Hamirpur	1.93	1.54	1.56	1.93	1.39	0.39	7.49	7.10	1.58	1.99	5.26
	Kangra	1.88	1.56	1.64	1.01	1.00	0.60	4.24	3.64	1.56	0.80	−0.36

Abbreviations: GM: geometric mean; SD: standard deviation; R: range; Sk: skewness; IQR: interquartile range; ϰ: kurtosis.

in the east containing yellowish brown oxidized and whitish grey homogeneous sandstone rocks. No significant variations in the activity concentration of ^{232}Th were observed in the studied region. Fig. 2(h) as given in (Table 1). The overall mean activity concentration of ^{40}K was also homogeneous; however, its magnitude was higher due to the excessive feldspar in the Siwalik area. Quartz and feldspar (plagiocase and K feldspar respectively) species are uniformly distributed in the rocks and gradually increase the ^{40}K concentration in this region. ^{226}Ra and ^{40}K isotopes exhibited almost uniform patterns of increasing concentrations towards Dhuli Bhatawan (south) and decreasing concentrations along DhanotaNala (east) as shown in Fig. 2(h and i). ^{232}Th has the same distribution with high concentrations along Manawala and low concentrations towards Dhuli Bhatawan consisting of grey sandstone and feldspar (Kothari et al., 2017). The results of petrological studies revealed that the radioactive samples obtained from the GamirKhad and Dhul areas contained ferruginous silty shales and shaly siltstones; they were composed of silt size clasts of quartz and feldspar mixed with a ferruginous clay matrix. To examine the relationship between the radionuclides, Kendell tau correlation was derived. The Kendell tau correlation coefficients determined for ^{226}Ra, ^{232}Th and ^{40}K species indicated a weak correlation between the activity concentrations of ^{226}Ra and ^{232}Th ($r = 0.152$, $p < 0.05$). No significant correlations were observed between the ^{232}Th and ^{40}K concentrations ($r = 0.013$, $p < 0.05$) and between ^{226}Ra and ^{40}K concentrations ($r = 0.004$, $p > 0.05$). The results are in agreement with those observed in Singhbhum shear zone (Chakraborty et al., 2009). In previous studies, various correlations between the concentrations of these radionuclides were obtained due to their different origins and rock type parameters (Kovacs et al., 2013; Hassan et al., 2018).

In Una, positively skewed frequency distributions deviating from normality were observed for activity concentrations of ^{226}Ra ($S = 2.48$, $ϰ = 6.10$), ^{232}Th ($S = 5.71$, $ϰ = 47.85$) and ^{40}K ($S = 9.65$, $ϰ = 105.31$), which represented general trends for naturally occurring radionuclides (Table 1). Similar positively skewed data was observed for Hamirpur and Kangra. S–W tests were conducted to identify the normality distributions of these radionuclides. The obtained p values were lower than 0.05 corresponding to non-normal distributions; however, the logarithmic transformation of the skewed data demonstrated normal distributions (the p value observed for lognormal transformed data points obtained by S–W testing were greater than 0.05) as shown in Table S5. Fig. S1 demonstrate the normal and log-transformed histogram plots of ^{226}Ra, ^{232}Th and ^{40}K activity concentrations in the studied region; the latter graph confirmed the normality of the statistical distribution of the obtained data points around their mean values.

The ratio of the mean value of ^{226}Ra activity to that of ^{232}Th activity was 8.8 for Una, 12.8 for Kangra, and 15 for the Hamirpur region due to uranium mineralization. The samples were collected at shallow depths between 20 and 30 cm and intercepted the mineralization. Further, the high disequilibrium factor (^{238}U/^{226}Ra) suggests that the process of uranium mineralization was still in the dynamic state and that uranium species were constantly moved from the clay-oxidizing zone and precipitated leading to the enrichment of the reduced zone.

The overall migration of ^{226}Ra was observed towards Hamirpur (south east) which is due to the soil being alluvial having large pores, low absorption characteristics and easy flow in watery structures (Aközcan et al., 2018).

3.1.2. Spatial distribution of the gamma dose rate

Gamma exposure rates at the sample sites were measured in μR/hr using scintillometer. These exposure rates were converted to AEDE using an outdoor occupancy factor of 0.2. The results of average absorbed dose rate level in the Una, Hamirpur, and Kangra

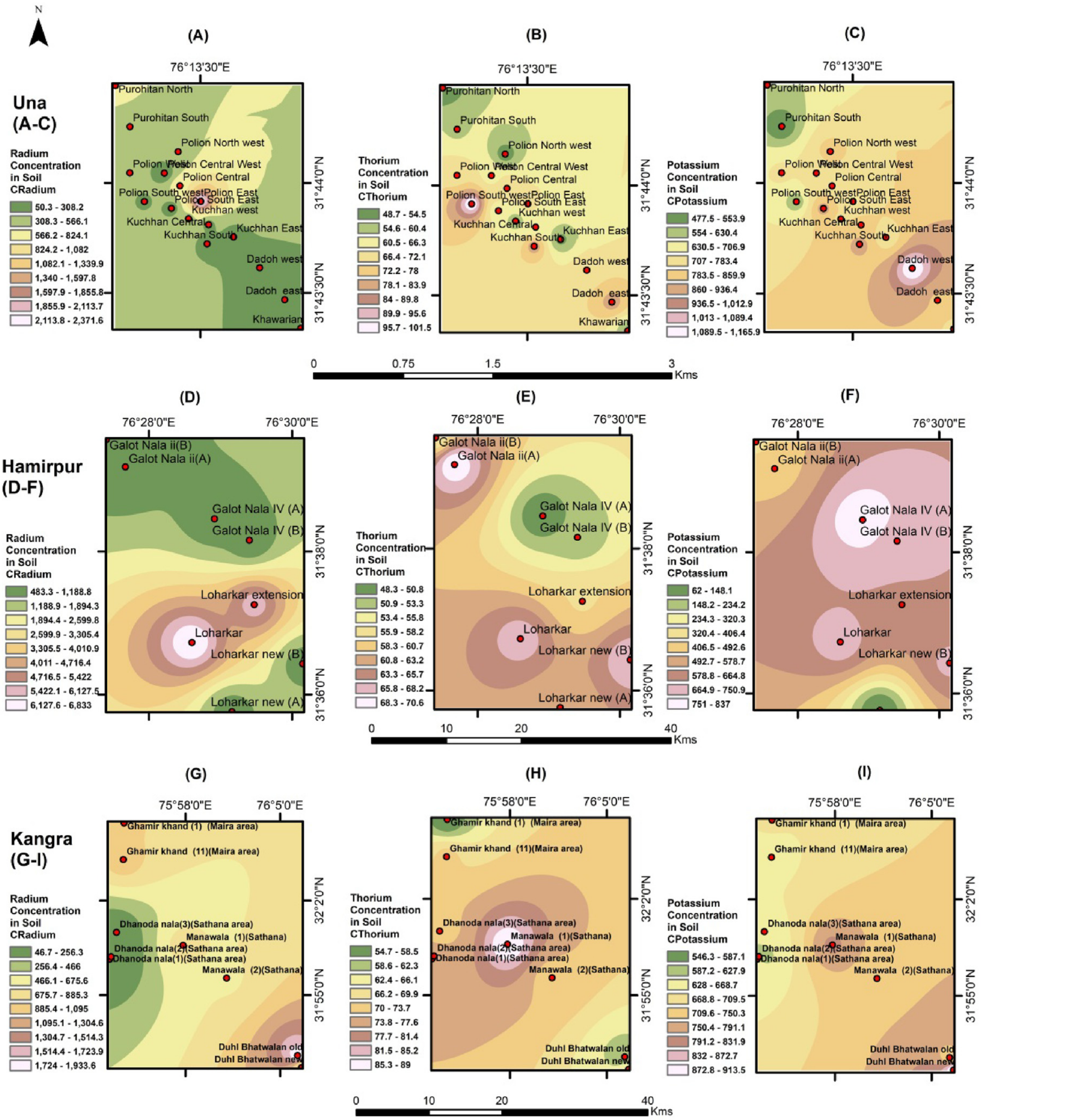

Fig. 2. Spatial distribution of activity concentration (Bq kg $^{-1}$)(a) ^{226}Ra, (b) ^{232}Th and (c) ^{40}K radionuclides in Una district.(d)^{226}Ra (e) ^{232}Th and (f) ^{40}K radionuclides in Hamirpur district.(g) ^{226}Ra, (h) and ^{23}2Th and (i) ^{40}K in Kangra district.

regions were 118, 163, and 135 nGyh^{-1} respectively (Fig. 3(a)). A positive correlation (R^2 = 0.63) was observed between the measured dose rate in field and calculated dose rates from grab samples (Fig. 3(b)). This is in agreement with other reports (Achola et al., 2012; Srinivas et al., 2017). The air absorbed dose rate measured from the grab samples were relatively higher when compared to that measured 1 m above the air, as the samples were collected from mineralized zone.

The annual effective dose due to activity (AEDE) in the soil is calculated using the following equation (United Nations Scientific Committee on the Effect of Atomic Radiation (UNSCEAR), 2000).

$$AEDE\left(mSv\, y^{-1}\right) = D\left(nGy\, h^{-1}\right) \times 8760\, h \times 0.2 \times 0.7\left(Sv\, Gy^{-1}\right)$$

The annual effective dose has been calculated in the studied area using the conversion convention (0.7 Sv Gy^{-1}) and occupancy factor (20% for outdoor occupancy Factor) as discussed by UNSCEAR (United Nations Scientific Committee on the Effect of Atomic Radiation (UNSCEAR), 2000; UNSCEAR, 2008), 8760 is the time in hours.

The results of annual effective dose were 0.15, 0.20 and 0.16 mSv

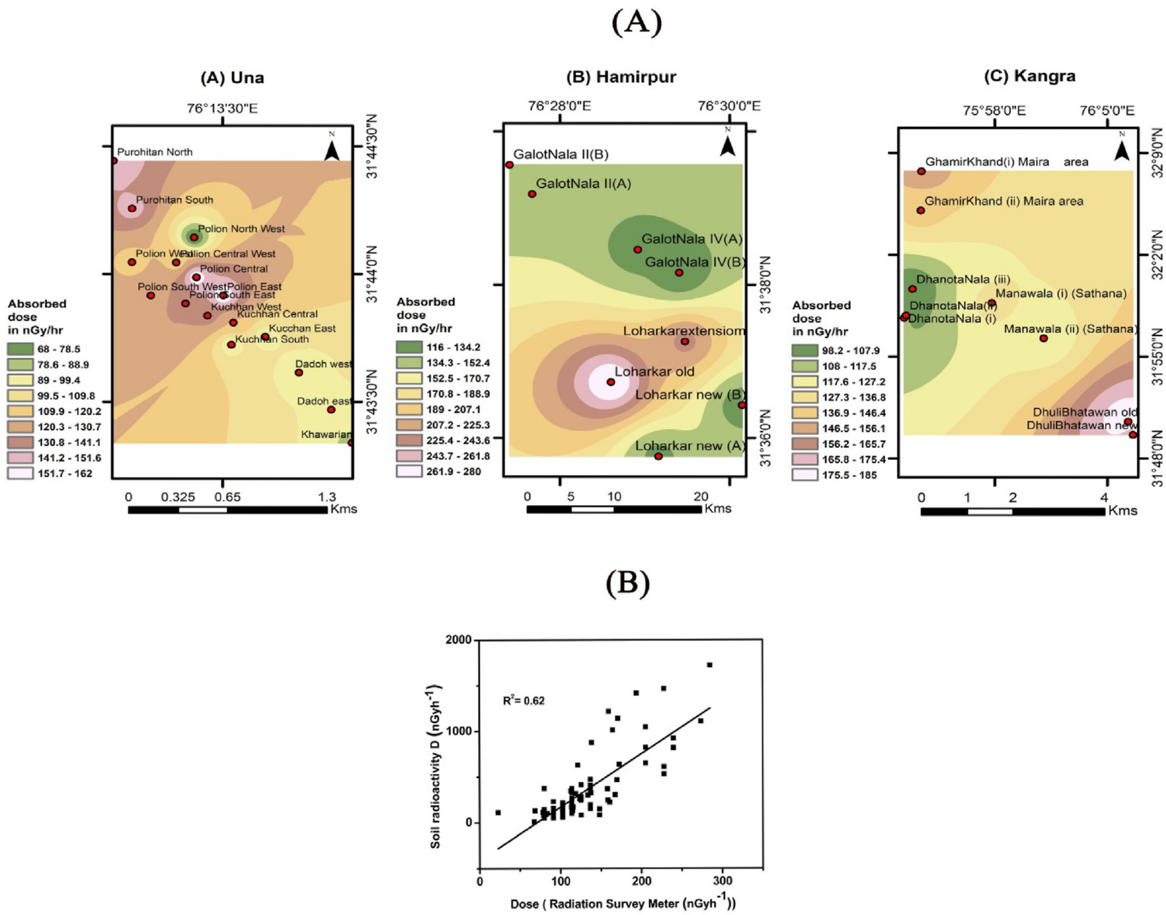

Fig. 3. Spatial distribution of (a) Gamma dose rate (nGy h^{-1}) (b) Correlation between measured and calculated gamma dose rate.

in Una, Hamirpur and Kangra respectively. The measurement is affected by the mineralization near the soil (around 1 m from the topsoil) and radius of 10 m around its location. So the total dose rate is generated by the integration near a concentrated mineralized zone (around 1 m) and a distributed non mineralized zone (10 m).

3.1.3. Radiological hazard parameter

The statistical characteristics of the radiological hazard indices are listed in Table 1. The D(nGyh^{-1}) measured in the Una, Hamirpur, and Kangra regions ranged from 52.7 to 1722 nGy h^{-1}, from 87.9 to 1741.3 nGy h^{-1} and from 135.2 to 985.6 nGy h^{-1} respectively. These results are in good agreement with that observed in the higher atomic mineral occurrences Dharmapuri Shear zone (Tamil Nadu, India) by Bhattacharya et al. (2018), in Jaduguda region (Maharana et al., 2011) and in Lambwe East Kenya (Achola et al., 2012). The average indoor and outdoor dose equivalents in the Una, Hamirpur, and Kangra regions were 1.33 and 0.33, 2.2 and 0.55 and 2.14 and 0.53 mSv y^{-1} respectively. The % contributions of ^{226}Ra, ^{232}Th and ^{40}K radionuclides to the total dose in Una, Hamirpur and Kangra was 78.8, 12.0, 9.1; 86.2, 7.7, 6.1 and 84.1, 8.8 and 7.1 respectively. The world average % contribution of ^{226}Ra, ^{232}Th and ^{40}K to the total dose is 25%, 40% and 35%.

The primary objective of measuring $H_{ex}$is to limit the radiation exposure caused by natural radionuclides to a permissible limit of 1 mSv y^{-1}. The mean values of H_{ex}determined for the Una, Hamirpur, and Kangra regions were 1.58, 2.61 and 2.37 while the corresponding mean values of H_{in}were 2.74, 4.83 and 4.37 respectively. These magnitudes are greater than their standard unity values indicating that the soil in these regions is unsafe for construction purposes according to the European Commission of Radiation Protection (European Commission on Radiation Protection (ECRP), 1999). The I_{γ}parameter is used to estimate the γ value – the radiation hazard level of soil samples. The magnitudes of I_{γ}determined for the Una, Hamirpur, and Kangra regions ranged from 0.83 to 25.01, from 1.38 to 25.31 and from 1.38 to 14.35, respectively (Table 1). The values of $I_{\gamma}\leq$ 0.5 correspond to the dose rate criterion of 0.3 mSv y^{-1}; while $I_{\gamma}\geq$ 0.5 correspond to the dose rate criterion of 1 mSv y^{-1}. ELCR values were calculated to assess the additional risk of developing cancer due to the exposure to toxic substances acquired over the lifetime. Their magnitudes obtained for the Una, Hamirpur, and Kangra regions were $(0.21–7.3) \times 10^{-3}$, $(0.39–7.49) \times 10^{-3}$ and $(0.39–4.24) \times 10^{-3}$ respectively. The ELCR risk was higher than the world average of 0.29×10^{-3} (United Nations Scientific Committee on the Effect of Atomic Radiation (UNSCEAR), 2000). The spatial distribution of Ra_{eq}, H_{ex} , H_{in} and ELCR is shown in Fig. 4.

3.1.4. Multivariate statistical analysis

Factor analysis (FA) was performed to classify the similar variables. The variables used for this analysis were ^{226}Ra, ^{232}Th, ^{40}K, D(nGyh^{-1}), AEDE, I_{γ}.H_{in} , H_{ex}, ELCR. Dimension reduction was performed and it was found that Kaiser-Meyer-Olkin (KMO) and Bartlett's test of sphericity was significant (KMO = 0.78 > 0.6, p = 0.00 < 0.005) and entails sample adequacy. Further χ^2 = 10967.46 was found significant at p < 0.05 (Table S6). Factor analysis yielded two factors with eigen value > 1 explaining 88% of

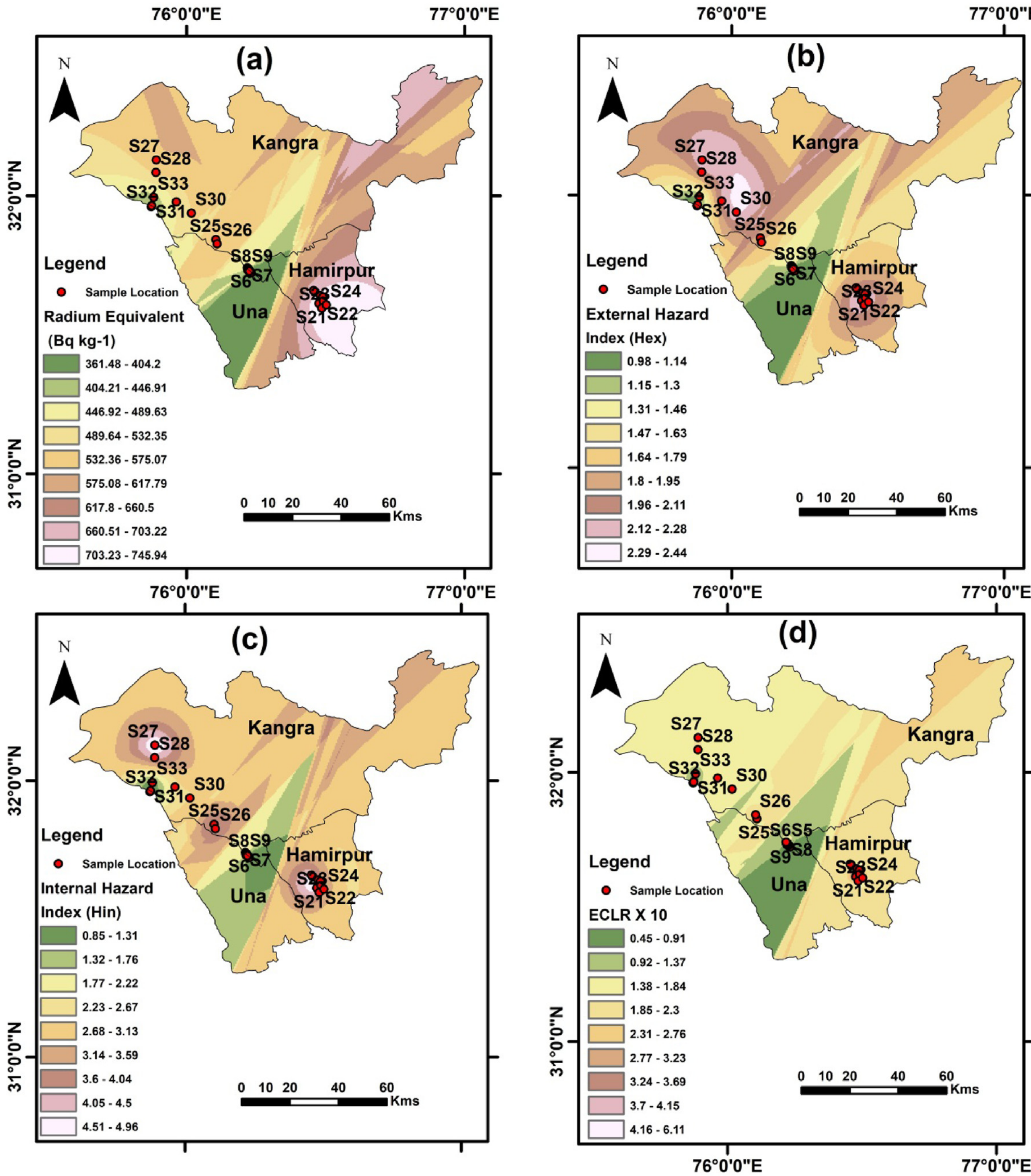

Fig. 4. Spatial activity distribution of **(a)** Radium equivalent **(b)** External Hazard Indices **(c)** Internal Hazard Indices (d) ELCR in districts of Una, Hamirpur and Kangra.

the total variance. On examining the rotated component matrix ^{232}Th was found to load almost equally on the two factors, and the magnitude of loading was less than 0.3. Therefore, it does not account for any common factor and has to be eliminated from the final factor solution. Out of the other 8 variables, ^{40}K loaded on a single factor while rest of the 7 items loaded on the other factor. This indicated that ^{40}K is not correlated with the other variables and constitutes a separate factor within the current sample of soil having various concentrations of elements. This ^{40}K factor accounts for 12.5% of variance, compared to 75.4% variance by the other factor. The first factor consists of ^{226}Ra, AEDE, D(nGyh-1), H_{ex} , H_{in}, and I_{γ} which are significant radioactive hazards in the soil sample.

3.2. Heavy metal analysis

3.2.1. Heavy metal concentrations

Descriptive statistics obtained for six priority metals (Cr, Ni, Co, Cu, Zn, and Pb) in the soil samples collected from each region and its comparison with the global data is provided in Table 2. The average heavy metal concentrations in the Una region followed the trend Zn (53.19) > Pb (53)> Ni (25)> Cr (21)> Cu (19.4)> Co (18.7) mg/kg respectively. The average background values of Cr, Ni, Cu, Zn, Pb and Co were 22, 26.3, 23, 49.04, 49.85 and 22 mgkg^{-1} respectively. In Hamirpur region the contents of Cr, Ni, Cu, Zn, Pb and Co exceeded the reference background values by 1.25, 1.20, 1.81, 1.54, 1.61 and 1.64 times respectively. Similarly, the contents of these metals in the Kangra region were greater than the average

Table 2
Statistical parameters of heavy metals (Cr, Ni, Cu, Zn, Pb and Co) in the Una, Hamirpur and Kangra region.

		Cr	Ni	Cu	Zn	Pb	Co
Una Region	Min	17	18	15	44	45	14
	Max	30	34	25	66	58	27
	Mean	21.88	25	19.44	53.19	53	18.69
	Median	20	24	19	52	53.50	17.50
	GM	21.40	24.61	19.17	52.81	52.85	18.37
	Std. Dev	4.938	4.938	3.326	6.635	4.082	3.719
	CV	0.2257	0.2257	0.1711	0.124	0.077	0.199
	Skewness	0.959	0.959	0.120	0.606	−0.638	0.957
	Kurtosis	−0.763	−0.141	−0.181	−0.751	−0.516	0.021
	MAD	4.078	3.5	2.70	5.46	3.25	2.984
Hamirpur Region	Min	20	23	28	53	57	58
	Max	34	35	50	100	117	42
	Mean	27.5	29.75	41.75	75.5	80.125	35.5
	Median	27	31	43	74	76	35.5
	GM	27.10	29.39	40.967	74.217	78.37	35.13
	Std. Dev.	4.898	4.83	8.22	14.81	18.64	4.78
	CV	0.1784	0.162	0.1969	0.1962	0.232	0.1367
	Skewness	−0.121	−0.363	−0.729	0.223	1.0688	0.120
	Kurtosis	−1.195	−1.743	−0.726	−0.0733	1.428	−0.356
	MAD	4.0	4.062	6.5	11.2	13.65	3.5
Kangra Region	Min	22	35	31	45	40	28
	Max	40	56	55	104	70	44
	Mean	28.22	43.77	41	69.3	56.7	38.7
	Median	25	43	37	50	55	40
	GM	27.55	43.05	40	65.2	55.5	38.3
	Std. Dev.	6.76	8.54	9.8	25.9	12.3	5.04
	CV	0.239	0.195	0.24	0.373	0.216	0.310
	Skewness	0.813	0.451	0.46	0.345	-.08	−1.29
	Kurtosis	−0.955	−1.76	−1.57	−2.30	−2.06	1.5
	MAD	5.629	–	8.51	23.9	10.86	3.78
	Indian natural soil background[a]	114	27.7	56.5	22.1	13.1	15.2
	Indian limit for soil[b]	–	–	135–270	300–600	250–500	–
	Poland soil guidelines[c]	150	100	150	300	100	20
	China soil guideline[d]	200	50	100	250	300	–
	Average background values in China[e](CNEMC)	61	26.9	22.6	74.2	26	–
	CNEMC[f]	61.00	26.90	–	74.20	26.00	–
	CEPC[g]	200.00	100.00	–	250.00	120.00	–

[a] Kumar et al., 2019, Gowd et al., 2010.
[b] Awasthi 2000.
[c] Wcislo 2012.
[d] NEPA 1995.
[e] Chen 2015.
[f] CNEMC (China National Environmental Monitoring Centre) 1990.
[g] CEPC (Chinese Environmental Protection Administration)2018.

Table 3
Linear regression between heavy metals and sediment physicochemical properties in Una, Hamirpur and Kangra district.

		Si β P	Al_2O_3 β P	Mn_2O_3 β P	Fe_2O_3 β P	Clay β P	OM β P	PH β p	R^2
Una	Cr	- -	- -	- -	0.544 [b]	0.32 [b]	.41 [c]	- -	0.35
	Co	−0.28 [c]	0.28 [c]	- -	0.75 [c]	0.15 [c]	0.32 [b]	- -	0.73
	Ni	−0.32 [c]	- -	- -	- -	- -	0.07 [a]	- -	0.54
	Cu	- -	0.34 [c]	- -	0.55 [b]	0.43 [a]	0.43 [a]	0.27 [b]	0.57
	Zn	0.50 [b]	0.72 [b]	0.18 [c]	0.35 [b]	0.15 [c]	0.21 [b]	- -	0.82
	Pb	0.82 [b]	0.96 [b]	- -	0.57 [c]	0.31 [b]	0.53 [b]	- -	0.77
Hamirpur	Cr	0.31 [c]	- -	- -	0.61 [b]	0.25 [a]	0.38 [c]	- -	0.40
	Co	−0.32 [b]	- -	- -	0.72 [b]	- -	0.57 [b]	- -	0.51
	Ni	−0.45 [b]	0.51 [c]	0.43 [c]	0.59 [c]	0.33 [b]	- -	- -	0.37
	Cu	- -	- -	0.52 [b]	0.25 [b]	0.05 [b]	0.60 [c]	- -	0.61
	Zn	0.14 [c]	0.20 [b]	0.61 [b]	0.51 [b]	0.17 [c]	- -	- -	0.42
	Pb	0.25 [c]	0.14 [c]	054 [c]	0.40 [b]	0.13 [a]	0.75 [b]		0.53
Kangra	Cr	−0.20 [c]	0.15 [c]	0.13 [b]	0.43 [b]	0.15 [b]	013 [a]	- -	0.40
	Co	0.31 [b]	0.20 [b]	0.20 [b]	0.27 [b]	0.05 [b]	0.21 [c]	- -	0.73
	Ni	0.25 [c]	0.16 [b]	- -	0.14 [a]	0.13 [b]	0.33 [c]	- -	0.53
	Cu	0.42 [c]	0.05 [b]	- -	0.25 [a]	0.36 [a]	0.16 [b]	- -	0.48
	Zn	0.33 [c]	0.21 [a]	0.08 [a]	0.38 [b]	0.42 [c]	0.05 [b]	- -	0.53
	Pb	0.15 [c]	0.31 [b]	0.13 [b]	0.22 [b]	0.42 [c]	- -	- -	0.26

[a] $p < 0.001$ (correlation is significant at 0.001 level).
[b] $p < 0.01$(correlation is significant at 0.01 level).
[c] $p < 0.05$ (correlation is significant at 0.05 level0.

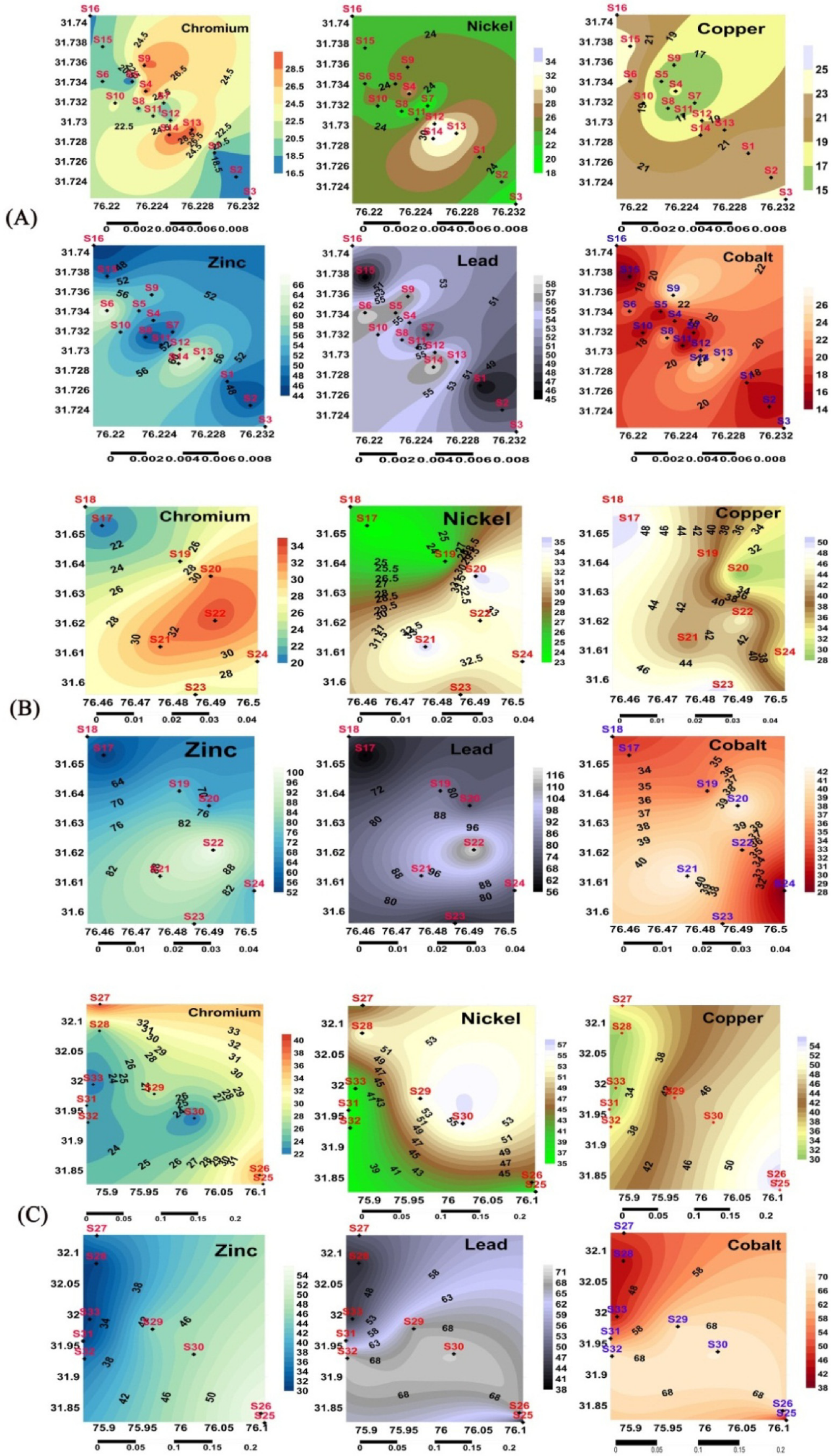

Fig. 5. Spatial distribution of heavy metals concentration Cr, Ni, Cu, Zn, Pb and Co (mg/kg) in Una, Hamirpur and Kangra region.

background values by 1.28, 1.64, 1.76, 1.41, 1.13 and 1.75 times respectively. Elevated high concentration of heavy metals in this region is due to thick layer of organic content and high clay content. In Hamirpur and Kangra similar type of trend was obtained, while in Una region concentrations of heavy metals were varied. In the present study, the mean contents of Cr, Ni, and Cu were lower, whereas those of Pb, Zn and Co exceeded the average Indian background values (Gowd et al., 2010). In addition, the concentrations of heavy metals were lower than the risk screening levels established for the residential and industrial land uses of Polish, Canadian and Chinese soils (Table 2) (Awasthi, 2000; Wcislo, E., 2012; CNEMC , 1990).

Coefficient of variation (CV) is a key statistical parameter for identifying anthropogenic sources from geogenic activities. In Una, Cr, Cu, Zn, Pb and Co species exhibited low variability's, and their CVs ranged from 7% to 19%, whereas Ni demonstrated a 22% variation. These results indicate that soil contamination in the studied area can be attributed to natural or lithogenic sources. For Hamirpur and Kangra regions, the corresponding CV magnitudes obtained for heavy metals were close to 30% suggesting the dominance of natural processes with anthropogenic influences.

All heavy metals in the study regions exhibited normal distribution patterns with ($-1 < S_k < 1$) and kurtosis ($-2 < K < 2$) which were validated by performing S–W tests ($p > 0.05$). Two sample *t*-test conducted to determine the differences in the means of the datasets obtained for the heavy metals of Una, Hamirpur, and Kangra indicated sufficient evidence to reject the null hypothesis at 95% confidence interval ($p < 0.05$) and that the means of the three regions were significantly different.

3.2.2. *Multivariate statistical analysis (for source identification)*

The results of linear regression between heavy metals and sediment physico-chemical properties are indicated in Table 3. In Una, the Cr showed a positive correlation between Fe_2O_3 ($p < 0.01$), organic matter ($p < 0.05$) and clay content ($p < 0.01$). Co was negatively correlated to Si ($p < 0.05$), mildly positively correlated to Al_2O_3 ($p < 0.05$), clay content ($p < 0.05$) and organic matter ($p < 0.01$) and strongly positively correlated to Fe_2O_3 ($p < 0.05$). Cu was positively correlated to Fe_2O_3 ($p < 0.01$), clay ($p < 0.001$) and organic matter ($p < 0.01$). Zn was strongly positively correlated to Al_2O_3 ($p < 0.01$) and mildly positively correlated to Fe_2O_3 ($p < 0.05$), Mn2O3 ($p < 0.01$), clay ($p < 0.01$) and organic matter ($p < 0.01$). Pb was strongly positively correlated to Al_2O_3($p < 0.01$) and Fe_2O_3 ($p < 0.05$) and mildly positively correlated to clay ($p < 0.01$) and organic matter ($p < 0.01$). No significant correlation of the heavy metals with pH was observed. The pH varied from neutral (7.5) in Una to mildly alkaline (9.0) in Hamirpur and Kangra districts.

For source identification of heavy metals, Principal component analysis (PCA) was performed as the first step of a cluster analysis (CA) procedure. In Una, the KMO value (0.62) and results of Bartlett's test of sphericity ($p < 0.001$) showed that PCA could be used for data analysis. The eigenvalues of components PC1 = 3.029 and PC2 = 1.311 were greater than unity. According to the obtained Varimax rotation data, the values of PC1and PC2 explained 72% of the total variance. In particular, PC1 explained 53% of the variance and a strong positive loading for Cr, Ni, Pb, Zn, and Co suggesting their similar origins (Table S7 and Fig. S2). The main soil minerals in Una were plagioclase, montmorriollite and quartz which featured high concentration of SiO_2, Fe_2O_3, Al_2O_3, Mn_2O_3 and CaO. Fe_2O_3 is known to influence the correlation of other heavy metals such as Cu, Zn and Pb by its adsorptive capacity (Marchand et al., 2016). The results of linear regression analysis have indicated a positive correlation between Fe_2O_3 and Cr, Co, Cu, Zn and Pb which explained their geogenic nature. The second group demonstrated a strong positive loading for Cu (0.957) indicating different origin sources

Table 4
Inhalation, ingestion, and dermal uptake doses, hazard quotient, hazard indices for non-carcinogenic risk and carcinogenic risk of heavy metals in the studied region.

Region	Metals	Children ($mg\ kg^{-1}\ day^{-1}$)			Non-carcinogenic risk				Carcinogenic risk
		$Dose_{ing}$	$Dose_h$	$Dose_{derm}$	H_{ing}	H_h	H_{derm}	HI	
Una Region	Cr	2.8×10^{-4}	7.9×10^{-9}	2.4×10^{-7}	4.3×10^{-2}	2.8×10^{-4}	4.0×10^{-3}	9.6×10^{-2}	3.2×10^{-8}
	Co	2.3×10^{-4}	6.7×10^{-9}	2.1×10^{-7}	1.2×10^{-2}	1.2×10^{-3}	1.3×10^{-5}	1.3×10^{-2}	5.6×10^{-9}
	Ni	3.2×10^{-4}	8.19×10^{-9}	2.7×10^{-7}	1.6×10^{-2}	4.4×10^{-7}	5.5×10^{-5}	1.6×10^{-2}	6.4×10^{-10}
	Cu	2.5×10^{-4}	6.9×10^{-9}	2.1×10^{-7}	6.2×10^{-3}	1.7×10^{-7}	1.8×10^{-5}	6.2×10^{-3}	
	Zn	6.9×10^{-4}	1.9×10^{-8}	5.8×10^{-7}	2.3×10^{-3}	6.4×10^{-8}	9.7×10^{-6}	2.3×10^{-3}	
	Pb	6.8×10^{-4}	1.9×10^{-8}	5.8×10^{-7}	1.9×10^{-1}	5.8×10^{-6}	1.1×10^{-3}	1.9×10^{-1}	4.9×10^{-7}
Hamirpur Region	Cr	3.5×10^{-4}	9.8×10^{-9}	3.8×10^{-7}	1.1×10^{-1}	3.4×10^{-3}	5.0×10^{-3}	1.2×10^{-1}	3.5×10^{-8}
	Co	4.5×10^{-4}	1.3×10^{-8}	3.9×10^{-7}	2.3×10^{-2}	2.2×10^{-3}	2.5×10^{-5}	2.5×10^{-2}	1.1×10^{-8}
	Ni	3.8×10^{-4}	1.1×10^{-8}	3.3×10^{-7}	1.9×10^{-2}	5.2×10^{-7}	6.5×10^{-5}	1.9×10^{-2}	7.7×10^{-10}
	Cu	5.3×10^{-4}	1.5×10^{-8}	4.6×10^{-7}	1.3×10^{-2}	3.7×10^{-7}	3.8×10^{-5}	1.3×10^{-2}	
	Zn	9.6×10^{-4}	2.7×10^{-8}	8.3×10^{-7}	3.2×10^{-3}	8.9×10^{-8}	1.4×10^{-5}	3.2×10^{-3}	
	Pb	1.0×10^{-3}	2.9×10^{-8}	8.8×10^{-7}	2.9×10^{-1}	8.8×10^{-6}	1.7×10^{-3}	2.9×10^{-1}	7.5×10^{-7}
Kangra Region	Cr	3.3×10^{-4}	1.0×10^{-8}	3.1×10^{-7}	1.1×10^{-1}	3.5×10^{-4}	5.7×10^{-3}	1.2×10^{-1}	3.6×10^{-8}
	Co	4.9×10^{-4}	1.4×10^{-8}	4.2×10^{-7}	2.5×10^{-2}	2.4×10^{-3}	2.6×10^{-5}	2.7×10^{-2}	1.2×10^{-8}
	Ni	5.6×10^{-4}	1.6×10^{-8}	4.8×10^{-7}	2.8×10^{-2}	7.6×10^{-7}	9.6×10^{-5}	2.8×10^{-2}	1.1×10^{-9}
	Cu	5.2×10^{-4}	1.4×10^{-8}	4.5×10^{-7}	1.3×10^{-2}	3.6×10^{-7}	3.7×10^{-5}	1.3×10^{-2}	
	Zn	8.9×10^{-4}	2.5×10^{-8}	7.6×10^{-7}	2.9×10^{-3}	8.3×10^{-8}	1.3×10^{-5}	3.0×10^{-3}	
	Pb	7.83×10^{-4}	2.0×10^{-8}	6.2×10^{-7}	2.0×10^{-1}	6.2×10^{-6}	1.2×10^{-3}	2.1×10^{-1}	5.3×10^{-7}

Region	Metals	Adults ($mg\ kg^{-1}\ day^{-1}$)			Non-carcinogenic risk				Carcinogenic risk
		$Dose_{ing}$	$Dose_h$	$Dose_{derm}$	Hq_{ing}	Hq_{inl}	Hq_{derm}	HI	
Una Region	Cr	3.3×10^{-5}	4.5×10^{-9}	3.2×10^{-8}	1.0×10^{-2}	1.6×10^{-4}	5.3×10^{-4}	1.1×10^{-2}	6.4×10^{-8}
	Co	2.5×10^{-5}	3.8×10^{-9}	2.7×10^{-8}	1.3×10^{-3}	6.5×10^{-4}	1.7×10^{-6}	1.9×10^{-3}	1.3×10^{-8}
	Ni	3.4×10^{-5}	5.1×10^{-9}	3.7×10^{-8}	1.7×10^{-3}	2.5×10^{-7}	6.8×10^{-6}	1.7×10^{-3}	1.5×10^{-9}
	Cu	2.6×10^{-5}	3.9×10^{-9}	2.8×10^{-8}	6.6×10^{-4}	9.6×10^{-8}	2.4×10^{-6}	6.7×10^{-4}	
	Zn	7.4×10^{-5}	1.1×10^{-8}	7.8×10^{-8}	2.5×10^{-4}	3.6×10^{-8}	1.3×10^{-6}	2.4×10^{-4}	
	Pb	7.2×10^{-5}	1.1×10^{-8}	7.8×10^{-8}	2.1×10^{-2}	3.3×10^{-5}	1.5×10^{-4}	2.1×10^{-2}	2.1×10^{-7}
Hamirpur Region	Cr	3.8×10^{-5}	5.5×10^{-9}	4.0×10^{-8}	1.3×10^{-2}	1.9×10^{-4}	6.7×10^{-4}	1.3×10^{-2}	2.3×10^{-7}
	Co	4.8×10^{-5}	7.1×10^{-9}	5.2×10^{-8}	2.4×10^{-3}	1.2×10^{-3}	3.2×10^{-6}	3.7×10^{-3}	2.4×10^{-8}
	Ni	4.1×10^{-5}	5.9×10^{-9}	4.4×10^{-8}	2.0×10^{-3}	2.9×10^{-7}	8.1×10^{-6}	2.0×10^{-3}	5.0×10^{-9}
	Cu	5.7×10^{-5}	8.4×10^{-9}	6.1×10^{-8}	1.4×10^{-3}	2.1×10^{-7}	5.1×10^{-6}	1.1×10^{-3}	
	Zn	1.0×10^{-4}	1.5×10^{-8}	1.1×10^{-7}	3.4×10^{-4}	5.0×10^{-8}	1.8×10^{-6}	3.5×10^{-4}	
	Pb	1.1×10^{-4}	1.6×10^{-8}	1.0×10^{-8}	2.1×10^{-1}	5.0×10^{-5}	2.0×10^{-5}	2.0×10^{-1}	9.3×10^{-7}
Kangra Region	Cr	3.9×10^{-5}	5.7×10^{-9}	4.1×10^{-8}	1.3×10^{-2}	2.0×10^{-4}	6.9×10^{-4}	1.4×10^{-2}	8.1×10^{-8}
	Co	5.3×10^{-5}	7.8×10^{-9}	5.7×10^{-8}	2.6×10^{-3}	1.4×10^{-3}	3.5×10^{-6}	4.0×10^{-3}	2.6×10^{-8}
	Ni	5.9×10^{-5}	8.8×10^{-9}	6.4×10^{-8}	3.0×10^{-3}	4.3×10^{-7}	1.2×10^{-5}	3.0×10^{-3}	2.5×10^{-9}
	Cu	5.6×10^{-5}	8.2×10^{-9}	6.0×10^{-7}	1.4×10^{-3}	2.0×10^{-7}	6.0×10^{-5}	1.4×10^{-3}	
	Zn	9.4×10^{-5}	1.4×10^{-8}	1.0×10^{-7}	3.2×10^{-4}	4.6×10^{-8}	1.7×10^{-6}	3.2×10^{-4}	
	Pb	7.8×10^{-5}	1.1×10^{-8}	8.3×10^{-8}	1.5×10^{-1}	3.5×10^{-5}	1.6×10^{-4}	1.5×10^{-1}	2.3×10^{-7}

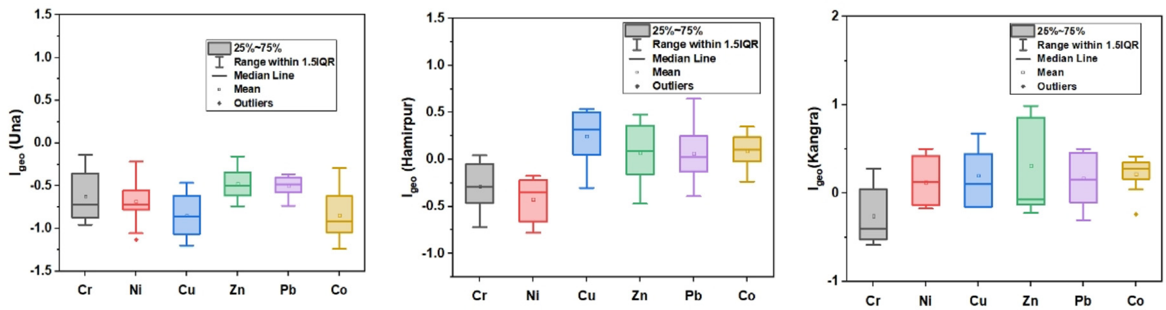

Fig. 6. Box Plots of I_{geo} in Una, Hamirpur and Kangra region.

explaining 18% of variation. Linear regression analysis indicated a positive correlation between Cu and Al_2O_3 explaining its geogenic origin.

Pearson correlation coefficient analysis also revealed the existence of significant positive correlations ($p < 0.05$) between various heavy metals: Pb and Zn ($r = 0.694$), Ni and Cr ($r = 0.622$), Zn and Ni ($r = 0.608$), Co and Zn ($r = 0.510$) and Co and Pb ($r = 0.584$) (Table S8). Hence, the FA results are in good agreement with the Pearson correlation coefficient. Hierarchical cluster analysis (HCA) results presented in the dendogram showed that two distinct groups were observed in Una (Fig. S3). Zn and Pb elements belong to the first cluster; the second cluster is divided into different subgroups constituting Ni, Cu, Co and Cr.

The FA data obtained for Hamirpur revealed two groups with strong positive loadings for Zn, Pb and Cr metals suggesting similar origin sources in the first group. In the second group, strong positive loading for Ni (0.816) and negative loading for Cu (−0.919) indicated their different sources of origin, that explained 20.3% of variation (Table S9, Fig. S4). Pearson correlation coefficient indicated a strong positive correlation between Pb and Cr ($r = 0.799$) and Zn and Cr ($r = 0.783$). A positive correlation was observed between Zn and Pb ($r = 0.855$) and Ni and Cr ($r = 0.875$). The data was statistically significant at ($p < 0.01$) and ($p < 0.05$) (Table S10). The cluster analysis of heavy metals in Hamirpur is depicted in Fig. S5. For Kangra region, a negative correlation existed between Co and Cr ($r = -0.803$) and a strong positive correlation between Cu and Zn ($r = 0.931$). These results matched the PCA data where Co and Cr constituted PC1 with a strong positive loading for Cr (0.949) and a negative loading for Co (−0.868). The results of the multivariate statistical analyses conducted for Kangra are provided in Table S11 – S12.

3.3. Spatial distributions of heavy metals

The hazard caused by the heavy metal in soil depends not only on the concentration, but also on their mobility, speciation and bioavailability (Salazar et al., 2012). The spatial distributions of heavy metals (Cr, Co, Cu, Ni, Zn, and Pb) are shown separately for each studied region (Fig. 5). In Una region, the obtained geochemical maps revealed relatively high concentrations of Cr, Zn, Co, Ni and Pb at the S_4 (Polian central), S_9 (Polian northwest), S_6 (Polian west) and S_{14} (Kuchhan south) sampling sites. The spatial distribution of the majority of heavy metals in Una was related mainly to the Fe/Mn oxides, clay content and organic matter. The % of sand and mud (silt and clay) was in ratio 70:30 in Una, (40:60) in Hamirpur and (50:50) in Kangra. Organic matter occurred as clots, stringers and fine laminae in sandstone. The organic matter varied from 5% in Una to 17% in Hamirpur and 10% in Kangra. The Fe_2O_3 concentration and organic content was higher in central region (S_4) and (S_9) due to higher thickness of mudbed and decreases towards S_1. Fine mudstone (having silt and clay) retain organic matter and Fe_2O_3, which attaches the heavy metals due to complexation (Zhu et al., 2019). Significant correlation of Cr, Zn and Pb with Fe_2O_3 and mudstone is observed as indicated by the results of regression analysis. These conditions leaded to high concentration of heavy metals in the central portion of Una. In contrast, Cu showed mildly high concentration in north western and south eastern part. Regression analysis has showed a positive correlation between Cu and Al_2O_3. The results of spatial distribution are in corroboration with multivariate statistical analysis.

In the Hamirpur region, significant metal loadings existed due to the additional variations related to the anthropogenic activities pertaining to previous mining. The organic content at Hamirpur was (17%) which strengthens the soil adsorption capacity for heavy minerals hence the sites at S_{22} and S_{21} were having higher concentration of Co, Cr, Ni, Zn, Co and Pb whereas high Cu concentration was observed at S_{17} and S_{23} sites. In Hamirpur, the heavy metals are positively correlated to Fe_2O_3 as indicated by regression analysis. The natural source of iron is ferruginous silty shale. The enhanced concentration of Zn and Pb in the S_{21} and S_{22} region was as also attributed to the former mining activity Kangra has a larger terrain and its spatial distributions were dependent on greater slope, geogenic and anthropogenic factors. Kangra had rich organic content which showed increase towards the south east portion towards Dhuli Bhatawan. S_{25} and S_{26} represented high priority sites for Cr, Cu, Zn, Co, and Pb which showed migration towards south east. Low concentration of heavy metals was observed at S_{31}, S_{32} and S_{33} whereas Ni exhibited the opposite pattern with an enhancement in the central portion.

3.3.1. Human health risk assessment

For non-carcinogenic health risk (HQ) assessment, the average daily dose of exposure ($Dose_{ing}$, $Dose_h$ and $Dose_{derm}$) and hazard quotients ((H_{ing}, H_h, and H_{derm}) corresponding to different pathways were calculated separately for children and adults as tabulated in Table 4. For the adults living in the Una region, the H_{ing} values obtained for heavy metals followed the pattern Pb (2.1×10^{-2}) > Cr (1.0×10^{-2}) > Ni (1.7×10^{-3}) > Co (1.3×10^{-3}) > Cu (6.6×10^{-4}) > Zn (2.5×10^{-4}). The H_h magnitudes were arranged in the sequence Co (6.5×10^{-4}) > Cr (1.6×10^{-4}) > Pb (3.3×10^{-5}) > Ni (2.5×10^{-7}) > Cu (9.6×10^{-8}) > Zn (3.6×10^{-8}), whereas H_{derm} exhibited the trend of Cr (5.3×10^{-4}) > Pb (1.5×10^{-4}) > Ni (6.8×10^{-6}) > Cu (2.4×10^{-6}) > Co (1.7×10^{-6}) > Zn (1.3×10^{-6}). In the Una region, the H_{ing}, H_h and H_{derm} magnitudes obtained for children followed the patterns Pb > Cr > Ni > Co > Zn > Cu, Co > Cr > Pb > Ni > Cu > Zn, and Cr > Pb > Ni > Cu > Co > Zn, respectively. The $Dose_{ing}$ in the studied region was 3–4 orders of magnitude greater than $Dose_h$ and $Dose_{derm}$ values due to the direct

Table 5
Heavy metal pollution indices (I_{geo}), EF, $PI_{nemerow}$, RI and CSI calculated on the basis of heavy metal content in Una, Hamirpur and Kangra region.

		Igeo			EF			RI			RItot	PInemerow			CSI		
		MEAN	MIN	MAX	MEAN	MIN	MAX	MEAN	MIN	MAX	MEAN	MEAN	MIN	MAX	MEAN	MIN	MAX
Una Region	Cr	−0.62	−0.95	−0.14	1.007	0.756	1.36	1.988	1.545	2.72	17.81	0.6205	0.5323	0.7359	2.24	1.84	2.90
	Ni	−0.68	−1.13	−0.22	0.955	0.749	1.251	0.9494	0.6836	1.291							
	Co	−0.845	−1.24	−0.29	0.86	0.60	1.20	4.247	3.181	6.136							
	Cu	−0.85	−1.20	−0.46	0.860	0.638	1.192	4.225	3.260	5.43							
	Zn	−0.48	−0.74	−0.16	1.095	0.880	1.334	1.08	0.897	1.34							
	Pb	−0.50	−0.73	−0.37	1.075	0.8522	1.233	5.31	4.51	5.81							
Hamirpur Region	Cr	−0.2838	−0.722	0.0430	1.355	1.00	1.629	2.409	1.818	3.0909	30.398	1.2959	0.9552	1.7030	2.2799	1.65109	3.162
	Ni	−0.4264	−0.788	−0.17	1.225	0.96	1.572	1.08241	0.87352	1.3292							
	Co	0.0937	−0.237	0.3479	1.747	1.596	2.012	8.06818	6.3636	9.5454							
	Cu	0.247	−0.301	0.645	2.004	1.138	2.801	9.5652	6.08695	10.869							
	Zn	0.07366	−0.4729	0.4755	1.674	1.189	2..150	1.48858	1.08075	2.0391							
	Pb	0.067	−0.237	0.3479	1.756	1.258	2.475	7.7858	5.717	11.735							
Kangra Region	Cr	−0.260	−0.58496	0.2775	1.3959	1.17506	1.7641	2.5656	2	3.636	29.0634	1.00174	0.77414	1.2364	2.433	1.873	3.2806
	Ni	0.12467	−0.1743	0.5037	1.846	1.280	2.515	1.6626	1.329	2.1268							
	Co	0.2164	−0.2370	0.41503	1.270	0.7512	1.762	8.8859	4.8832	16.913							
	Cu	0.2008	−0.15432	0.6728	1.9353	1.5311	2.519	8.840	6.739	11.9565							
	Zn	0.3115	−0.222	0.9861	1.5436	0.8903	2.234	1.4138	0.9176	2.1207							
	Pb	0.16602	−0.3074	0.4999	1.9610	1.2347	2.3549	5.6998	4.0120	7.0210							

and most common exposure pathway. The HQ values in the Una region determined for adults and children were in the order of Pb > Cr > Co > Ni > Cu > Zn and Pb > Cr > Ni > Co > Cu > Zn, respectively. In case of both adults and children, the HQs of Pb and Cr contributed to 90% of the HI values. In Hamirpur and Kangra regions, the HQ magnitudes obtained for adults and children followed the sequence Pb > Cr > Co > Ni > Cu > Zn, in which Pb and Cr were major contributors to HI. In the Hamirpur region, the total HI values determined for adults and children were 2.3×10^{-1} and 4.7×10^{-1}, respectively. Similarly, in the Kangra region, the HI values for adults and children were 1.7×10^{-1} and 3.95×10^{-1}, respectively. The HI child-to-adult ratios determined for the Una, Hamirpur, and Kangra regions were 9.5, 2.0, and 2.3, respectively. Because the HI values in studied regions were less than unity, the non-carcinogenic risks estimated for both adults and children were within the acceptable limits (The children in studied areas were found to be more susceptible to non-carcinogenic risks than the adults).

The carcinogenic risk (CR) is defined as the incremental probability of developing cancer in human beings due to exposures to potential carcinogens. CR and total carcinogenic risk (TCR) values in the studied region were estimated using the methodology outlined in Table S4. The dose is multiplied by the corresponding slope factor (SF) to produce CR (Ferreira-Baptista and De Miguel, 2005). Based on the classification criteria of IARC (International Agency for Research on Cancer) and IRIS (Integrated Risk Information System) out of the four elements, Cr, Ni, and Co are considered carcinogen by inhalation, while Pb is considered carcinogen by ingestion (IARC, 2011; IRIS, 2013). The mean (10–90%) values of TCR obtained for adults and children in the Una region were 2.9×10^{-7} and 5.3×10^{-7} respectively. In the Hamirpur region, the TCR magnitudes determined for adults and children were 1.2×10^{-6} and 7.8×10^{-7}, while in the Kangra region, the values were 3.37×10^{-7} and 1.12×10^{-8}, respectively (Table 4). Because the TCR values ranged from 1×10^{-8} to 1×10^{-6}, no significant CR was identified for adults and children. The observed carcinogenic risk was greater for children than for adults due to the higher ingestion rate. A similar CR pattern (Pb > Cr > Co > Ni) was observed for adults and children in all three regions.

3.3.2. *Environmental risk assessment using geochemical indicators*

The box plots of I_{geo} values obtained for the heavy metals in the studied region are presented in Fig. 6 (their magnitudes vary from −1.3 to 1). Table 5 depicts the descriptive statistics of I_{geo}, EF, $PI_{nemerow}$, RI and CSI. The magnitude of I_{geo} was computed for each metal using its average normal background (mgkg^{-1}). Almost 83% of I_{geo} values obtained for Cr, 84% for Ni, 67% for Cu, 64% for Pb, and 58% for Co corresponded to unpolluted sites (I_{geo}<0). Since the average I_{geo} magnitudes in the Una region for all heavy metals (I_{geo}<0) hence, heavy metals in that region did not pose any significant contamination risk. The minimum I_{geo} value in Una was observed at S_{16} (−1.237) and maximum I_{geo} value was observed at S_4 (−0.137). Moderate degrees of pollution were obtained for Pb, Cu, Co, and Zn in Hamirpur and Kangra ($0 < I_{geo} < 1$). The minimum I_{geo} value was observed at S_{17} (−0.7800), and the maximum one at S_{23} (0.5353) in the Hamirpur region. The minimum I_{geo} in Kangra was −0.5849 and the maximum I_{geo} was 0.9861. The highest I_{geo} variations were observed for Zn, Co, and Pb. Around 15% of I_{geo} values obtained for Ni, 30% for Pb, 27% for Cu, 27% for Zn and 33% for Co corresponded to sites that were moderately polluted with these metals.

An EF-based approach was used to differentiate between the elements produced by natural phenomena and human activities. Fe was utilized as the reference element due to its widespread

Table 6
Comparative chart of I_{geo} and EF of cities around the world.

	Cr	Ni	Cu	Zn	Pb	Co	Location	References
Igeo	−0.62	−0.68	−0.85	−0.48	−0.50	−0.85	Una	Present Study
	−0.28	−0.43	0.24	0.07	0.067	0.09	Hamirpur	Present study
	−0.26	0.12	0.20	0.31	0.17	0.22	Kangra	Present Study
	0.4	0.4	1.5	0.9	4.3	–	China	Gu et al. (2016)
	2.0	2.4	1.0	1.0	2.3	–	Greece	Papazotos et al. (2016)
	0.2	0.3	1.5	1.4	7.9	–	Brazil	Figueiredo et al. (2007)
	0.5	0.4	1.7	2.2	7.9	–	Beijing, China	Du et al. (2013)
EF	1.0	0.96	0.86	1.1	1.1	0.86	Una	Present stdy
	1.3	1.2	2.0	1.7	1.8	1.7	Hamirpur	Present study
	1.4	1.8	1.9	1.5	2.0	1.3	Kangra	Present Study
	5.99	7.30	9.55	6.59	4.02	–	India	Kumar et al. (2019)
	0.4	4.0	5.1	2.8	7.0	–	Poland	Charzyński et al. (2017)
	4.2	5.0	2.2	0.0	5.0	–	Greece	Papazotos et al. (2016)
	0.8	0.8	3.3	0.0	9.3	–	China	Gu et al. (2016)
RI	1.98	0.94	4.2	1.08	5.3	4.2	Una	Present study
	2.4	1.08	9.5	1.48	7.7	8.06	Hamirpur	Present study
	2.5	1.6	8.8	8.4	5.7	8.8	Kangra	Present Study
	9.22	28.10	36.73	5.07	15.47	–	India	Kumar et al. (2019)
	2.98	6.88	7.62	1.64	7.51	–	Northern plateau of spain	Santos-Francés et al. (2017)

presence and its insusceptibility to anthropogenic activities. In Una region, the average EF values of Cr, Ni, Cu, Zn, Pb, and Co were 1.19, 1.26, 1.43, 1.36, 1.29, and 1.38 respectively. However, the mean EF values obtained in the Hamirpur region for Cu (2.004), Zn (1.674), Pb (1.756), and Co (1.747) and in the Kangra region for Ni (1.85), Cu (1.94), Zn (1.54), and Co (1.97) were greater than 1.5 suggesting anthropogenic influences. Generally, EF magnitudes between 0 and 1.5 indicated that the metal might originate from a crustal material or a natural weathering process. In Hamirpur and Kangra regions, the average EF values determined for Cr were less than 1.5, whereas the mean EF values obtained for Cu, Zn and Co were slightly greater than 1.5, which could be attributed to anthropogenic activities. A total of 27% sites containing Cu, 6% sites containing Pb, 6% sites containing Ni, 12% sites containing Zn, and 15% sites containing Co found to be moderately contaminated. Previous studies have shown that Cu is major contaminants of mineral and mining resources, which is consistent with the data presented in this work (Kumar et al., 2019). Relatively high EF values were observed at the S_{26}, S_{22}, and S_{23} sites and minimal enrichment was observed at S_{15}. Zn and Pb are chemical elements that are introduced into the environment mainly by the natural weathering of their ore deposits (Table 5). Table 6 represents the comparison of the I_{geo} and EF with the values across the world.

Pollution due to multiple heavy metals was comprehensively evaluated using the $PI_{nemerow}$ index. Based on the classification criteria, its magnitude varied from "unpolluted" in Una (0.6) to "low-level pollution" in the Hamirpur region (1.29). The main heavy metal pollutants included Pb, Co, and Cu. The distribution of $PI_{nemerow}$ in different regions is shown in Fig. 7. Almost 87.5% sites of Hamirpur and 55% of Kangra ($1< PI_{nemerow} <2$) were slightly polluted.

The toxicity response coefficients for Cr, Ni, Cu, Zn, Pb, and Co were 2, 5, 5, 1, 5, and 5, respectively (Håkanson, 1980). The ecological risks caused by individual elements followed the sequence Pb > Co > Cu > Cr > Zn > Ni in the Una region. In the case of the Hamirpur region, the sequence was Cu > Co > Pb > Cr > Zn > Ni. Finally, in the Kangra region, the trend was Co > Cu > Pb > Cr > Ni > Zn. The average RI values determined for the Una, Hamirpur, and Kangra regions were below 150 indicating low ecological risks (Table 5). The minimum RI value (15.7) was observed at S_2 whereas the maximum was observed at S_{23} (36.0) (Fig. 6). The comparative chart of ecological risk indices in

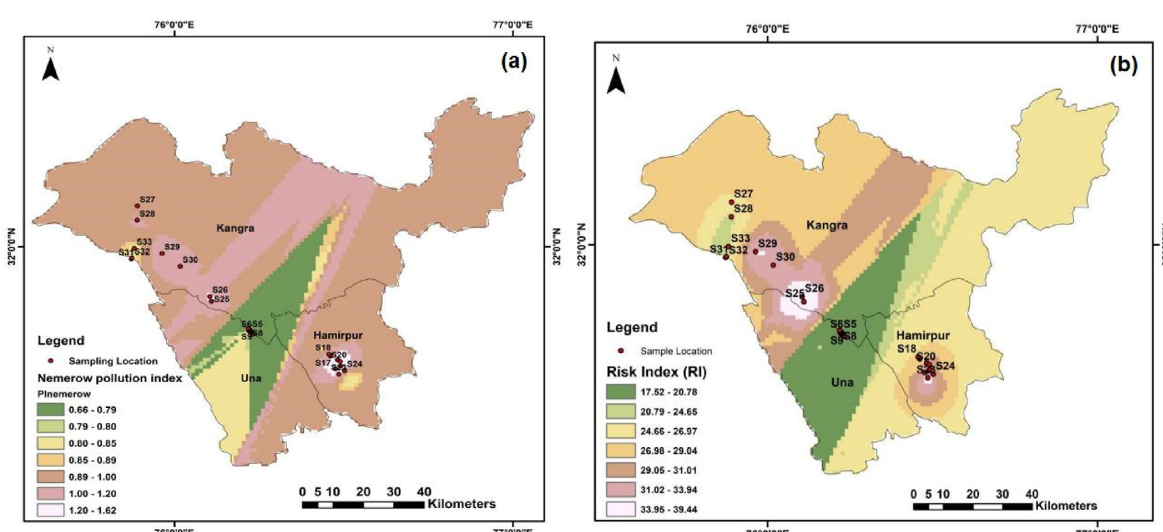

Fig. 7. Spatial distribution of (a) $PI_{nemerow}$ (b) RI in Una, Hamirpur and Kangra districts.

Table 7
Comparative chart of ecological risk indices $PI_{nemerow}$, RI and CSI of cities around the world.

RI	$PI_{nemerrow}$	CSI	Location	References
17.81	0.62	2.24	Una	Present Study
30.33	1.29	2.27	Hamirpur	Present Study
29.1	1.0	2.4	Kangra	Present Study
254.3	2.2	319.7	Xiamen Island (China)	Luo et al. (2012)
25.6	0.9	40.9	Asadabad(Iran)	Solgi (2016)
92.6	0.4	108.7	Faisalabad (Pakistan)	Parveen et al. (2012)
487.3	0.9	801.9	Belgrade (Serbia)	Kuzmanoski et al. (2014)

indicated in Table 7.

Furthermore, moderate to high values of CSI was observed in the Una (2.24), Hamirpur (2.28), and Kangra (2.43) regions. Note that CSI is a very sensitive index that shows relatively high contamination as compared with other indicators. As per CSI index almost 27% sites were having low to moderate severity, 45% were having moderate severity and 6% were having high severity contamination index.

4. Conclusion

The present manuscript described the concentration, spatial distribution, environmental health risk and pollution risk from radionuclides and the heavy metals in the uranium mineralized region of Siwaliks. The average activity concentration of radionuclides (^{226}Ra, ^{232}Th and ^{40}K) as well as the radiological hazard parameters was higher than recommended safe limits by United Nations Scientific Committee on the Effect of Atomic Radiation (UNSCEAR) (2000). The highest radiological contamination was observed at Loharkar old (S_{21}) followed by Loharkar extension (S_{22}), Dhuli Bhatawan (S_{25}) and Polion East (S_7). This implies that highly mineralized uraniferrous zone is responsible for radiological risk .^{40}K and ^{232}Th scanty contributed to radiological risk in the studied region. Cluster analysis method identified ^{226}Ra to be primarily contributing radionuclide, hence specific strategy is required to ameliorate the environmental impact of radiological contamination. The average air absorbed dose rates measured for the Una, Hamirpur, and Kangra regions were 118, 163, and 135 $nGyh^{-1}$ which was higher compared to the world average of 69 $nGyh^{-1}$. Further too comprehensively assess the effect of pollution risk, the heavy metal contamination was studied using pollution indices. The sites with the highest contamination were S_{21} (Loharkar old), S_{22} (Loharkar extension), $S_{26,}$ (Dhuli Bhatawan old), S_{27} (GhamirKhand) and S_{16}. (Purohitan North). The abundance and migration of heavy metals in Siwaliks were governed by geogenic factors. The obtained I_{geo} data and corresponding EF magnitudes suggested that Co, Pb, and Cu were major pollutants. The estimated eco-environmental risk indices as well as the RI, $PI_{nemerow}$, and CSI parameters showed that the study region was a low-risk zone. Information on soil pollution generated by geochemical and radiological mapping in Siwaliks indicated that uranium and heavy metals precipitated southward of the clay oxidizing zone. This study provided basic information on the concentrations, distributions and potential hazards of radionuclides and heavy metals in uranium mineralized region of Siwaliks and may help in formulating policies that can minimize the deleterious effect on human health and environment.

Declaration of competing interests

The authors declare no competing financial and non-financial interests.

Author credit statement

The study was conceptualized and designed by P. Pandit, V.kumar and P. Bangotra. Acquistion of the data was carried out by P. Pandit and D.Ghosh. Analysis and interpretation of the data was being done by P.Pandit, P, Mangla, V.Kumar, R.Mehra and P. Bangotra. Drafting of the manuscript was carried out by P. Pandit, V.Kumar, P.bangotra and R. Mehra.

Acknowledgements

Three of the authors are highly grateful to Shri. M. B. Verma, Director AMD for giving permission for pursuing this project.

Appendix A. Supplementary data

Supplementary data to this article can be found online at https://doi.org/10.1016/j.chemosphere.2020.126857.

Abbreviations

AMD	Atomic Minerals Directorate for Exploration and Research
AGRS	airborne and ground based radiometric survey
WDXRF	wavelength dispersive X-ray fluorescence
EF	enrichment factor; SPSS: Statistical Program for Social Science
S–W	Shapiro–Wilk
RSM	radiation survey meter
AEDE	annual effective dose equivalent
ELCR	excess lifetime cancer risk
CV	coefficient of variation
PCA	principal component analysis
CA	cluster analysis
HCA	hierarchical cluster analysis
FA	factor analysis
HQ	hazard quotient
HI	hazard index
CR	carcinogenic risk
TCR	total carcinogenic risk
RI	Hakanson's ecological risk index
CSI	contamination severity index
AM	arithmetic mean
G.M	geometric mean
R	range
$PI_{nemerow}$	Nemerow pollution index
D	air absorbed dose rate
H_{ex}	external hazard index
H_{in}	internal hazard index
I_{geo}	geoaccumulation factor
SD	standard deviation
IQR	interquartile range
UNSCEAR	United Nations Scientific Committee on the Effects of Atomic Radiation
Sn	supplementary information.

References

Achola, S.O., Patel, J.P., Mustapha, A.O., Angeyo, H.K., 2012. Natural radioactivity and external dose in the high background radiation area of Lambwe East, Southwestern Kenya. Radiat. Protect. Dosim. 152, 423–428. https://doi.org/10.1093/rpd/ncs047.

Aközcan, S., Külahcı, F., Mercan, Y., 2018. A suggestion to radiological hazards characterization of ^{226}Ra, ^{232}Th, ^{40}K and ^{137}Cs: spatial distribution modeling. J. Hazard Mater. 353, 476–489. https://doi.org/10.1016/j.jhazmat.2018.04.042.

Awasthi, S.K., 2000. Prevention of food alteration act no.37 of 1954. Central and State Rules as Amended for 1999. Ashoka Law House, New Delhi.

Bangotra, P., Mehra, R., Jakhu, R., Pandit, P., Prasad, M., 2019. Quantification of an alpha flux based radiological dose from seasonal exposure to ^{222}Rn, ^{220}Rn and their different EEC species. Sci. Rep. 9, 2515. https://doi.org/10.1038/s41598-019-38871-6.
Belayaeva, O., Pyuskyulyan, K., Movsisyan, N., Saghaelyan, A., Carlvalho, F.P., 2019. Natural radioactivity in urban soils of mining centers in Armenia: dose rate and risk assessment. Chemosphere. https://doi.org/10.1016/j.chemosphere.2019.03.057.
Beretka, J., Matthew, P.J., 1985. Natural radioactivity of Australian building materials, industrial wastes and by products. Health Phys. 48, 87–95. https://doi.org/10.1097/00004032-198501000-00007.
Bhattacharya, T., Madhavi Shankar, V., Ram Mohan Reddy, B., Thangavel, S., Sharma, P.K., 2018. Radioactivity levels in the atomic mineral occurrences along Dharmapuri shear zone in parts of vellore, krishnagiri, Dharmapuri and salem districts of tamilnadu, India. Appl. Radiat. Isot. 132, 135–141. https://doi.org/10.1016/j.apradiso.2017.11.028.
Chakraborty, A., Tripathi, R.M., Puranik, V.D., 2009. Occurences of NORM and 137Cs in soils of Singhbhum regions of eastern India and associated radiation hazard. Radioprotection 44, 55–68.
Charzyński, P., Plak, A., Hanaka, A., 2017. Influence of the soil sealing on the geoaccumulation index of heavy metals and various pollution factors. Environ. Sci. Pollut. Res. 24 (5), 4801–4811.
CNEMC (China National Environmental Monitoring Centre), 1990. The Background Values of Elements in Chinese Soils. China Environmental Science Press, Beijing (In Chinese).
Cuvier, A., Purcelot, L., Probst, A., Prunier, J., Roux, G.L., 2016. Trace elements and Pb isotopes in soils and sediments impacted by uranium mining. Sci. Total Environ. 566–567, 238–249.
Du, Y., Gao, B., Zhou, H., Ju, X., Hao, H., Yin, S., 2013. Health risk assessment of heavy metals in road dusts in urban parks of Beijing, China. Procedia. Environ. Sci. 18, 299–309.
European Commission on Radiation Protection (ECRP), 1999. Radiological protection principles concerning the natural radioactivity of building materials. Radiat. Prot. 112.
Ferreira-Baptista, L., De Miguel, E., 2005. Geochemistry and risk assessment of street dust in Luanda, Angola: a tropical urban environment. Atmos. Environ. 39, 4501–4512. https://doi.org/10.1016/j.atmosenv.2005.03.026.
Figueiredo, A.M.G., Camargo, S.P., Pavese, A.C., Gumiero, F.C., Enzweiler, J., Sigolo, J.B., 2007. Metal Assessment in Urban Park Soils in Sao Paulo Metal Assessment in Urban Park Soils in Sao Paulo,2007 International Nuclear Atlantic Conference- INAC 2007. Santos, SP, Brazil. September 30 -. (Accessed 5 October 2007).
Gasiorek, M., Kowalska, J., Mazurek, R., Pajak, M., 2017. Comprehensive assessment of heavy metal pollution in topsoil of historical urban park on an example of the planty park in Krakpw (Poland). Chemosphere 179, 148–158.
Gowd, S.S., Reddy, M.R., Govil, P.K., 2010. Assessment of heavy metal contamination in Jajmau (Kanpur) and Unnao industrial areas of the Ganga plains, UttarPradesh, India. J. Hazard Mater. 174 (1), 113–121.
Gu, Y.G., Gao, Y.P., Lin, Q., 2016. Contamnation ,bioaccessibilty and human healthy risk of heavy metals in exposed loam soils from 28 urban parks in southern China's largest city Guang Zhou. Appl. Geochem. 67, 52–58.
Håkanson, L., 1980. An ecological risk index for aquatic pollution control: a sedimentological approach. Water Res. 14, 975–1001. https://doi.org/10.1016/0043-1354(80)90143-8.
Hao, Y.J., Chang, Q.R., Li, L.H., Wei, X.R., 2014. Impacts of landform, land use and soil type on soil chemical properties and enzymatic activities in a Loessial Gully watershed. Aust. J. Soil Res. 52, 453–462, 10.1071/sr13202.
Hassan, N.M., Kim, Y.J., Jang, J., Chang, B.U., Chae, J.S., 2018. Comparative study of precise measurements of natural radionuclides and radiation dose using in-situ and laboratory γ-ray spectroscopy techniques. Sci. Rep. 8, 14115. https://doi.org/10.1038/s41598-018-32220-9.
IARC, 2011. International agency for research on cancer. In: Agents Classified by the IARC Monographs, vols. 1–102.
ICRP, 2017. Occupational intakes of radionuclides: Part 3. ICRP publication - 137. Ann. ICRP 46 (3/4).
IRIS, 2013. Integrated Risk Information System) of USEPA. IRIS assessment. https://cfpub.epa.gov/ncea/iris2/atoz.cfm.
Kaul, R., Khan, B.U., Khazanchi, B.M., Miglani, B.S., Mahadevan, T.M., 1979. Regional hydrogeochemical investigations for uranium in Siwalik belt of Himachal Pradesh and Punjab. Himal. Geol. 9, 773–785.
Kaul, R., Umamaheshwar, K., Chandrashekharan, S., Deshmukh, R.D., Swarnkar, B.M., 1993. Uranium mineralization in the Siwaliks of north western himalayan, India. J. Geol. Soc. India 41, 243–258.
Kothari, P.K., Rahaman, M.D., Ghosh, D., Sinha, K.K., 2017. Uranium Investigation in Siwalik Region. Annual Report Siwalik Investigation., Himachal Pradesh. Atomic Minerals Directorate for Exploration and Research (unpublished).
Kovacs, T., Szeiler, G., Fabian, F., Kardos, R., Gregoric, A., Vaupotic, J., 2013. Systematic survey of natural radioactivity of soil in Slovenia. J. Environ. Radioact. 122, 70–78. https://doi.org/10.1016/j.jenvrad.2013.02.007.
Kumar, V., Sharma, A., Kaur, P., Sidhu, G.P.S., Bali, A.S., Bhardwaj, R., Thukral, A.K., Cerda, A., 2019. Pollution assessment of heavy metals in soils of India and ecological risk assessment: a state-of-the-art. Chemosphere 216, 449–462. https://doi.org/10.1016/j.chemosphere.2018.10.066.
Kuzmanoski, M., Todorovic, M., Anicic-Urosevic, M., Rajsic, S., 2014. Heavy metal content of soil in urban parks of Belgrade. Hemodial. Int. 68, 643–651.
Li, Z.Y., Ma, Z.W., Kuijp, T.J., Yuan, Z.W., Huang, L., 2014. A review of soil heavy metal pollution from mines in China: pollution and health risk assessment. Sci. Total Environ. 843–853. https://doi.org/10.1016/j.scitotenv.2013.08.090, 468–469.
Luo, C., Liu, C., Wang, Y., Liu, X., Li, F., Zhang, G., Li, X., 2011. Heavy metal contamination in soils and vegetables near an e-waste processing site, south China. J. Hazard Mater. 186, 481–490. https://doi.org/10.1016/j.jhazmat.2010.11.024.
Maharana, M., Swarnkar, M., Chougaonkar, M.P., Mayya, Y.S., Sengupta, D., 2011. Ambient gamma radiation levels (indoor and outdoor) in the villages around Jaduguda (India) using card-based CaSO4: Dy TL Dosemeters. Radiat. Protect. Dosim. 143, 88–96. https://doi.org/10.1093/rpd/ncq355.
Marchand, C., Fernandez, J.M., Moreton, B., 2016. Trace metal geochemistry in mangrove sediments and their transfer to mangrove plants (New Caledonia). Sci. Total Environ. 562, 216–227. https://doi.org/10.1016/j.scitotenv.2016.03.206.
Mkandawire, M., Deudel, E.G., 2005. Accumulation of arsenic in Lemna gibba L. (duckweed) in tailing waters of two abandoned uranium mining sites in Saxony, Germany. Sci. Total Environ. 336 (1–3), 81–89. https://doi.org/10.1016/j.scitotenv.2004.06.002.
Muller, G., 1969. Index of geoaccumulation in sediments of the rhine river. Geojournal 2, 108–118.
Örgün, Y., Altınsoy, N., Şahin, S.Y., Güngör, Y., Gültekin, A.H., Karahan, G., Karacık, Z., 2007. Natural and anthropogenic radionuclides in rocks and beach sands from Ezine region (Çanakkale), Western Anatolia, Turkey. Appl. Radiat. Isot. 65, 739–747. https://doi.org/10.1016/j.apradiso.2006.06.011.
Papazotos, P., Chalkiadaki, O., Chatzistamatiou, E.A., Geogopoulos, G., Gkiouleka, I., Katsikis, I., Zygouri, E., Kelepertzis, E., Argyraki, A., 2016. Heavy metals in urban park soils from Athens,Greece. In: Proceedings of the 14th Intern. Conference, Thessaloniki, XLVIII. Bulletin of the Geological Society of Greece. May 2016.
Parveen, N., Ghaffar, A., Shirazi, S.A., Bhalli, M.N., 2012. A GIS based assessment of heavy metals contamination in surface soil of urban parks: a case study of Faisalabad City-Pakistan. Mondal. J. Geogr. Nat. Disaster 2e11. https://doi.org/10.4172/2167-0587.1000105.
Pejman, A., Bidhendi, G.N., Ardestani, M., Saeedi, M., Baghvand, A., 2015. A new index for assessing heavy metals contamination in sediments: a case study. Ecol. Indicat. 58, 365–373. https://doi.org/10.1016/j.ecolind.2015.06.012.
Popic, J.M., Salbu, B., Strand, T., Skipperud, L., 2011. Assessment of radionuclide and metal contamination in a thorium rich area in Norway. J. Environ. Monit. 13, 1730–1738. https://doi.org/10.1039/c1em10107b.
Saha, J.K., Selladurai, R., Vassanda Coumar, M.L., Dotaniya, M.L., Kundu, S., Patra, A.K., 2017. Soil Pollution an Emerging Threat to Agriculture. Springer, Singapore. https://doi.org/10.1007/978-981-10-4274-4.
Santos-Francés, F., Martínez-Graña, A., Zarza, C.Á., Sánchez, A.G., Rojo, P.A., 2017. Spatial distribution of heavy metals and the environmental quality of soil in the northern plateau of Spain by geostatistical methods. Int. J. Environ. Res. Publ. Health 14 (6), 568. https://doi.org/10.3390/ijerph14060568.
Saito, K., Jacob, P., 1995. Gamma ray fields in the air due to sources in the ground. Radiat. Protect. Dosim. 58, 29–45. https://doi.org/10.1093/oxfordjournals.rpd.a082594.
Salazar, M.J., Rodrigues, J.H., Nieto, G.L., Pignata, M.L., 2012. Effects of heavy metal concentration (Cd, Zn and Pb) in agricultural soils near different emission sources on quality, accumulation and safety in soybean [Glycine max (L.) Merill]. J. Hazard Mater. 233, 244–253.
Salmanighabeshi, S., Palomo-Marin, M.R., Bernalte, E., Rueda-Holgado, F., MiroRodriguez, C., Fadic-Ruiz, X., Vidal-Cortez, V., Cereceda-Balic, F., Pinilla-Gil, E., 2015. Long-term assessment of ecological risk from deposition of elemental pollutants in the vicinity of the industrial area of Puchuncavi-Ventanas, central Chile. Sci. Total Environ. 527–528, 335–343. https://doi.org/10.1016/j.scitotenv.2015.05.010.
Singh, U.K., Ramanathan, A.L., Subramanian, V., 2018. Groundwater chemistry and human health risk assessment in the mining region of East Singhbhum, Jharkhand, India. Chemosphere. https://doi.org/10.1016/j.chemosphere.2018.04.060.
Solgi, E., 2016. Contamination of two heavy metals in topsoils of the urban parks Asadabad, Iran 2013. Arch. Hyg. Sci. 5, 92–101.
Srinivas, D., Babu, V.R., Patra, I., Tripathi, S., Ramayya, M.S., Chaturvedi, A.K., 2017. Assessment of background gamma radiation levels using airborne gamma ray spectrometer data over uranium deposits, Cuddapah Basin, India – a comparative study of dose rates estimated by AGRS and PGRS. J. Environ. Radioact. 167, 1–12. https://doi.org/10.1016/j.jenvrad.2016.11.027.
Sutherland, R.A., 2000. Bed sediment-associated trace metals in an urban stream. Oahu. Hawaii. Environ. Geol. 39, 611–627.
United Nations Scientific Committee on the Effect of Atomic Radiation (UNSCEAR), 2008. Annex B -Exposures of the Public and Workers from Various Sources of Radiation. United Nations, New York.
U.S. Environmental Protection Agency US EPA, 1989. Risk Assessment Guidance for Superfund (RAGS). Human Health Evaluation Manual Part A[R] Volume I. Office of emergency and remedial response, Washington, DC [EPA/540/1-89/002].
Wu, J., Lu, J., Li, L., Min, X., Luo, Y., 2018. Pollution, ecological-health risks, and sources of heavy metals in soil of the northeastern Qinghai-Tibet Plateau. Chemosphere 201, 234–242. https://doi.org/10.1016/j.chemosphere.2018.02.122.
Zhang, M., He, P., Qiao, G., Hung, J., Yuan, X., Li, Q., 2019. Heavy metal assessment and surface sediments of the Subei Shoal, China : spatial distribution, source apportionment and ecological risk. Chemosphere 223, 211–222. https://doi.org/10.1016/j.chemosphere.2019.02.058.
Zhong, L., Liming, L., Jiewen, Y., 2010. Assessment of heavy metals contamination of

paddy soil in Xiangyin County, China. Symposium 4.1.2 Management and Protection of Receiving Environments, 19th World Congress of Soil Science, pp. 17–20. Soil Solutions for a Changing World 191 e 6 August 2010, Brisbane, Australia.

Zhu, H., Bing, H., Wu, Y., Zhou, J., Sun, H., Wang, J., Wang, X., 2019. The spatial and vertical distribution of heavy metal contamination in sediments of the Three Gorges Reservoir determined by anti-seasonal flow regulation. Sci. Total Environ. 664, 79–88. https://doi.org/10.1016/j.scitotenv.2019.02.016.